AI BASED BIAS COMPENSATION FOR TUNING FORK GYROSCOPE

A PROJECT REPORT

submitted by

ASWATHY AJAYAN
(Reg. No. TKM21EEII04)

to

the APJ Abdul Kalam Technological University
in partial fulfillment of the requirements for the award of the Degree

of

Master of Technology
in

Electrical and Electronics Engineering

with specialisation in

Industrial Instrumentation and Control

Department of Electrical and Electronics Engineering

TKM College of Engineering Kollam
Kollam - 691 005

MAY 2023

DECLARATION

I undersigned hereby declare that the project report entitled "**AI based bias compensation for Tuning Fork Gyroscope**", submitted for partial fulfillment of the requirements for the award of degree of Master of Technology in Electrical and Electronics Engineering with specialisation in Industrial Instrumentation and Control, of the APJ Abdul Kalam Technological University, Kerala is a bonafide work done by me under the supervision of *Prof.Sumayya Jaleel*, Project Internal Supervisor, Assistant Professor, Department of Electrical and Electronics Engineering, *Mr.Anish G S*, Project External Supervisor, Scientist Engineer 'SF', ISRO Inertial Systems Unit, Thiruvananthapuram, *Prof. Amal A.*, Project Co-ordinator, Assistant Professor, Department of Electrical and Electronics Engineering. This submission represents my ideas in my own words and where ideas or words of others have been included. I have adequately and accurately cited and referenced the original sources. I also declare that I have adhered to ethics of academic honesty and integrity and have not misrepresented or fabricated any data or idea or fact or source in my submission. I understand that any violation of the above will be a cause for disciplinary action by the institute and/or the University and can also evoke penal action from the sources which have thus not been properly cited or from whom proper permission has not been obtained. This report has not been previously formed the basis for the award of any degree, diploma or similar title of any other University.

Kollam
May, 2023

ASWATHY AJAYAN

DEPARTMENT OF ELECTRICAL AND ELECTRONICS ENGINEERING

TKM COLLEGE OF ENGINEERING KOLLAM-691005

CERTIFICATE

This is to certify that the project report entitled " **AI based bias compensation for Tuning Fork Gyroscope**" submitted by **ASWATHY AJAYAN**, **(Reg. No. TKM21EEII04)** of fourth semester to the APJ Abdul Kalam Technological University in partial fulfillment of the requirements for the award of the Degree of Master of Technology in Electrical and Electronics Engineering with specialisation in Industrial Instrumentation and Control, is a bonafide record of the Project done by her under our guidance and supervision. This report in any form has not been submitted to any other University or Institute for any purpose.

Prof.Sumayya Jaleel
Internal Project Supervisor
Assistant Professor
Department of Electrical & Electronics Engg
TKM College of Engineering Kollam

Mr.Anish G S
External Project Supervisor
Sci/Engr. 'SD'
OELGD, ISG, AIS
ISRO Inertial Systems Unit Thiruvananthapuram

Prof. Shanavas T. N
Associate Professor and PG Co-ordinator
Department of Electrical & Electronics Engg
TKM College of Engineering Kollam

Dr. Sabeena Beevi. K
Associate Professor and Head
Department of Electrical & Electronics Engg
TKM College of Engineering Kollam

ACKNOWLEDGEMENT

A lot of effort and hard work has been put into this project in course of its presentation. However, it would not have been possible without the kind support and help of many individuals and other sources. I would like to extend my sincere thanks to all of them. I take this opportunity to express my deep sense of gratitude and sincere thanks to all who helped me to complete this project report successfully.

I thank God Almighty for paving my way throughout the project. I thank *Dr. Sabeena Beevi. K*, Associate Professor and Head, Department of Electrical and Electronics Engineering and *Prof. Shanavas T. N*, PG Co-ordinator, Department of Electrical and Electronics Engineering for their support and help.I express my sincere thanks to *Dr. Imthias Ahamed T P.*, Head of Centre for Artificial Intelligence, for his valuable help.

I am greatly thankful to my internal project supervisor *Prof.Sumayya Jaleel*, Assistant Professor, Department of Electrical and Electronics Engineering, for her supervision, and helpful suggestions. I would like to express my special gratitude to my external project supervisor *Mr.Anish G S*, Scientist Engineer ’SD’, ISRO Inertial Systems Unit, Thiruvananthapuram, for her valuable guidance, supervision and support throughout the project. I am expressing my sincere thanks to *Prof. Amal. A*, Project Co-ordinator, Assistant Professor, Department of Electrical and Electronics Engineering for the positive criticism and valuable comments.

Finally I thank my parents and friends who directly and indirectly contributed to the successful completion of my project.

ASWATHY AJAYAN

ABSTRACT

A gyroscope is an inertial instrument which is used to determine the angle of orientation or the rate of rotation relative to an inertial frame of reference. This work emphasises on type of gyroscope called a tuning fork gyroscope (TFG), which operates on the principle of corolis effect. Due to factors such as gyroscope self-heating and, variations in ambient conditions, the performance of a high precision strapdown inertial navigation system (SINS) gets affected and the gyroscope bias varies. The characteristics of bias drift in TFGs and various methods to compensate for it must therefore be studied.We suggest using a Long Short-Term Memory (LSTM) neural network model based on Empirical Mode Decomposition (EMD) and Seasonal Decomposition to forecast bias compensation accurately.

The purpose of this work is to employ artificial intelligence to create and evaluate bias compensation for tuning fork gyroscopes. To determine the strength and degree of linear relationships between sets of data, different types of correlations are compared. Denoising is essential to improve system performance, and this can be achieved through various methods, such as seasonal decomposition and empirical mode decomposition (EMD). The denoised data, or trend, is fed individually into Long-Short Term Memory (LSTM) neural networks to further enhance their performance. LSTM neural networks are a suitable option for predicting time series data and can be used effectively for forecasting bias compensation using historical data.By using a hybrid EMD-LSTM predictive algorithm, bias prediction and sensor performance improvement can be achieved. The proposed seasonal decomposition-LSTM method and EMD-LSTM hybrid forecasting model outperforms traditional LSTM neural networks.

List of Figures

ABBREVIATIONS

SINS	Strapdown Inertial Navigation Systems
INS	Inertial Navigation system
IMU	inertial Measurement Units
TFG	Tuning Fork Gyroscope
AI	Artificial Intelligence
ML	Machine Learning
EMD	Empirical mode decomposition
IMF	Intrinsic Mode functions
LSTM	Long Short Term Memory

Chapter 1

INTRODUCTION

Over the past decade, significant advancements have been made in the field of guidance, navigation, and control, particularly in navigation sensors. However, due to the drift over time of inertial sensors such as gyroscopes and accelerometers, they have been combined with other sensors to increase their accuracy. The use of GPS has significantly improved navigation capabilities and has enabled low cost solutions to navigation problems, but additional sensors are still necessary due to GPS's limitations. Choosing a sensor is challenging due to the various benefits and drawbacks of different sensor technologies, and meeting high-performance demands while minimizing cost and size is crucial. The introduction of smaller sensors has made it possible to implement guidance, navigation, and control in applications that were previously thought to be unattainable, and many of these applications will require mass production at a lower cost.

An inertial navigation system (INS) is a technology that uses motion sensors like accelerometers and gyroscopes to constantly calculate the position, orientation, and velocity of a moving object without the need for external references. INS is commonly used in guided missiles, spacecraft, submarines, ships, and planes. Other terms like inertial measurement units (IMU) are also used to describe similar technologies. Inertial navigation systems can now be produced in compact and light sizes thanks to recent innovations. These developments have expanded the range of potential applications to incorporate fields like motion capture of people and animals.

To set up an inertial navigation system (INS), a computer and a module that contains motion sensing components such as accelerometers and gyroscopes are required. Initially, the INS is given the velocity and position from a different source such as a GPS receiver, human operator or satellite, and later computes its own adjusted velocity and position by utilizing data from the motion sensors. The INS does not require external references once it is initialized, enabling it to establish its own position, velocity, and orientation. INS can detect changes in a person's geographic location, velocity, and orientation through the calculation of linear and angular accelerations. It is resistant to jamming and deceit as it doesn't require external reference post-initialization. INS are utilized in a range of moving objects like guided missiles, submarines, planes, and spacecraft, but their implementation is limited by their complexity and expense.

To determine the angular velocity of a system in the inertial frame of reference, gyroscopes are utilized. By integrating the angular velocity starting from the system's initial orientation in the inertial frame, the current orientation of the system can be determined. However, the accelerometers are attached to the system and rotate with it, and hence, they are incapable of determining their own orientation. Thus, they can only measure the linear acceleration of the system relative to the moving system in the inertial reference frame. Nevertheless, to ascertain the linear acceleration of the system in the inertial reference frame, the current linear acceleration relative to the moving system and the system's current angular velocity are monitored. The appropriate kinematic equations are utilized to integrate the inertial accelerations, resulting in the system's inertial velocities. Finally, integrating again utilizing the original location as the initial condition determines the system's inertial position. Inertial navigation systems are subject to integration drift, a common problem.

Newton's laws of classical mechanics are essential in the operation of inertial navigation systems (INS). INS uses motion sensors, including accelerometers and gyroscopes, along with a computer to constantly determine the position, orientation, and velocity (speed and direction of movement) of a moving object, without relying on any external references. These sensors, especially gyroscopes, measure angular velocity, which is the change in rotational angle per unit of time. Gyroscopes use the laws of angular momentum conservation to measure or maintain orientation. They are used in a variety of devices such as space launch vehicles, ballistic missiles, orbiting satellites, compasses, and automatic pilots on ships and planes. There are different types of gyroscopes, including mechanical gyroscopes, MEMS gyroscopes, tuning fork gyroscopes, and Coriolis force and laser gyroscopes, among others, such as ring lasers and fiber optic gyroscopes, which operate on the Sagnac effect principle.

Sensors, like any other device, produce measurements that have some level of bias. The bias of the sensor is significantly influenced by the temperature of the sensor. To mitigate this source of error, most gyroscopes have a temperature sensor built-in. Calibration is necessary to correct the biases of the gyroscopes.Machine learning methods are applied to correct for the tuning fork gyroscope's bias. Bias is quantified in degrees per second. Gyroscopes are susceptible to bias instabilities, where the initial zero reading of the gyroscope will gradually shift over time due to built-in imperfections and noise. When the gyroscope is at rest, it produces output known as bias or zero point error. Bias changes progressively over time, and this fluctuation's standard deviation is referred to as drift, which serves as a metric for the properties of gyroscopes.

The process of bias compensation in tuning fork gyroscopes involves correcting any potential errors or biases present in the gyroscope's output measurements. This is typically accomplished through the use of algorithms or mathematical models that analyze the gyroscope's output data and detect any systematic errors or deviations from expected values. The main objective of bias compensation in tuning fork gyroscopes is to enhance the precision and dependability of the gyroscope's measurements, particularly in scenarios where accuracy and stability are crucial. Various techniques are used for bias compensation in tuning fork gyroscopes, including Kalman filtering, adaptive filtering, and approaches based on neural networks.

Artificial neural networks have become increasingly popular with the rise of deep learning. They are highly adaptable, organized, and capable of learning, making them a better option for predicting passenger flow in scenarios with complex and non-linear data. However, traditional neural network algorithms like back-propagation neural networks (BPN) have a slow convergence speed, which makes them less accurate in predicting bias compensation. Therefore, BPN is not suitable for predicting bias compensation.

In recent years, researchers have introduced several new deep neural network models to improve their ability to handle time series data. Recurrent neural networks (RNN) add the concept of sequence to enhance their capacity to handle time series data. RNN technology has been particularly successful in natural language processing (NLP) applications such as speech recognition and machine translation. To address the "gradient vanishing" issue in RNNs, Hochreiter Schmidhuber proposed the Long Short-Term Memory (LSTM) Neural Network in 1997. Research indicates that LSTM neural networks are effective in forecasting bias compensation.[1][2].

In order to improve the performance of the LSTM model, it is important to denoise the training data which contains noise. Various methods such as Seasonal decomposition and empirical mode decomposition (EMD) can be used for denoising. These methods can help to extract the trend from the data and improve the performance of the LSTM model. To analyze non-linear and non-stationary time series data, empirical mode decomposition (EMD) is used. EMD is the prior component of the Hilbert-Huang transform (HHT)[3]. EMD can divide the original data into a number of intrinsic mode functions (IMFs) without the need to establish any basis functions. EMD is a valuable tool since it is capable of analyzing data that is non-linear and non-stationary.

To address the challenge of non-linear and non-stationary time series data, a combination of the EMD approach [4]and LSTM neural networks can be used to improve the accuracy of bias compensation prediction in gyros. The suggested method entails utilizing EMD to break down the data into IMFs, which are then given to an LSTM neural network model to make predictions based on past data. This innovative EMD-LSTM hybrid prediction technique has the potential to produce more precise predictions for bias compensation in gyroscopes.

1.1 OBJECTIVES

- To Analyze the bias drift occuring in Tuning Fork Gyroscope(TFG).
- To develop and evaluate AI based bias compensation for Tuning Fork Gyroscope(TFG).
- To analyse the drift data of the sensors and experiment with different AI models so as to achieve a suitable model to compensate effectively when operating under different conditions.

1.2 SCOPE

The scope of bias compensation in gyros involves reducing the error or inaccuracy caused by various factors such as temperature, sensor flaws, and noise, which can result in a shift in the initial zero reading of the gyro over time. This error can be measured in degrees per second, and it can progressively change over time. The standard deviation of this fluctuation is known as drift, which is used to gauge the properties of the gyros. The bias compensation process involves calibrating the gyros to reduce the impact of these factors on the measurements. This is achieved through various methods such as machine learning techniques, which can be used to compensate for the bias in the tuning fork gyro.

This in tuning fork gyroscopes is focused on improving the accuracy and reliability of the measurements produced by these sensors, particularly in applications where precise and stable measurements are important. The process involves identifying and correcting any systematic errors or biases that may exist in the gyroscope's output data using various mathematical models or algorithms. There are several methods that can be used for bias compensation, including Kalman filtering, adaptive filtering, and neural network-based approaches. The aim of bias compensation in tuning fork gyroscopes is to enhance their overall performance and enable them to be used in a wider range of applications that require highly accurate and reliable measurements.

1.3 ORGANISATION OF REPORT

The report is divided into six chapters, with the first chapter being the Introduction that covers the general background, objectives, and organization of the report. The second chapter reviews the literature relevant to the project. The third chapter focuses on Tuning Fork Gyroscope, which is the main topic of study in the report. The methodology for bias compensation is discussed in chapter 5, along with the results. The final chapter is the conclusion.

Chapter 2

LITERATURE REVIEW

2.1 OVERVIEW

In this chapter, the literature review related to gyroscopes and their types, as well as the fundamentals of Tuning Fork Gyroscope (TFG) and the bias compensation methodology used in previous studies, is presented. The chapter also provides an overview of the advanced analysis and control techniques used for bias compensation in TFG. Moreover, the chapter discusses the temperature control strategy which is used to maintain temperature stability, and the limitations of using temperature control techniques in different ways are also discussed.

Recently, various practical gyroscopes have been developed, with the vibrating member typically being a string, bell, thin ring, or rod suspended at the nodes of the primary vibration mode. One significant advantage of these systems is that they eliminate the need for bearings or similar components to enable high-speed rotation of the gyro wheel relative to the case, which is a major issue with spinning wheel gyros.

Vibrating member gyros, which lack bearings, eliminate wear and inaccuracies associated with wear that are present in rotating wheel gyros. Furthermore, the lack of a bearing function in vibrating member gyros eliminates the main source of power consumption.In addition, vibrating member gyros have other advantages. They are less sensitive to linear accelerations than rotating wheel gyros and are therefore better suited to high acceleration environments. They can also accept virtually unlimited angular velocity inputs without design compromises that may decrease the accuracy of rotating wheel gyros The vibrating member gyro is not without its practical issues, though, as with all instruments. Specifically, a device that utilizes the Foucault principles requires a perfectly functioning vibrating component that doesn't lose amplitude due to energy loss. It should possess complete dynamic symmetry and have its plane of oscillation moving at a rate determined exclusively by the angular rotation of the instrument. Without a drive system to maintain the oscillation, no realistic instrument will be entirely symmetrical and the mechanical energy of vibration will dissipate.To aid in the design of a practical instrument, we need an analysis in which the errors present is a non-ideal instrument are quantitatively related to the mechanical imperfections that causes these errors.

A vibrating structure gyroscope (VSG) is a type of gyroscope that is low-cost and widely available. These gyroscopes are made from various vibrating materials, such as tuning forks, planar square beams, and oscillating disc structures. They operate by creating a carrier mode motion through resonance, and when the structure is rotated about an orthogonal axis to the linear motion produced by the carrier motion, Coriolis forces are generated. These forces are then applied along the final orthogonal axis, resulting in the response mode, which is the second mode of oscillation for the vibrating structure. The amplitude of the response mode's motion is inversely proportional to the applied rotation rate and is in phase with the carrier mode.

Vibrating structure gyroscopes, which are affordable and compact, can be used in various high-volume applications, such as vehicle navigation and platform stabilization. However, their limited bias stability restricts their use in applications requiring high accuracy. A significant challenge to their performance is the quadrature bias error, which arises due to imperfections in the vibrating structures' shape. This error causes oscillations in the response mode, even when the gyroscopes are not spinning and are in phase quadrature to the motion produced by applied rotation rates. The quadrature signal can be effectively rejected by precisely phased electronics, but strict constraints are necessary for the phase precision of the detecting system to recover the required rotation-induced signal. Improvements in performance are needed to make vibrating structure gyroscopes suitable for more accurate applications.

The fiber optic gyroscope (FOG) is a widely used inertial measurement unit (IMU) in the military and aerospace industries due to its small size, accuracy, and simplicity[5]. However, FOG drift caused by noise, such as temperature drift, can affect its accuracy and reduce the IMU's resolution accuracy. To compensate for FOG drift and improve navigation accuracy, researchers have proposed using different methods, such as a long short-term memory recurrent neural network (LSTM-RNN)[2] model and a real-time temperature change rate acquisition method based on moving average, artificial fish swarm algorithm (AFSA)[6] and back-propagation (BP) neural network, and a nonlinear prediction model based on least-square support vector machines (LS-SVM)[7].

The EMD-LSTM hybrid prediction model is preferred over the single LSTM prediction model for predicting non-stationary and non-linear data[3][8][4]. . The EMD approach is used to analyze such data, while LSTM neural networks are used to learn from previous data for time series prediction. Traditional signal processing methods are not suitable for non-stationary and non-linear signals, so time-frequency analysis techniques like the EMD algorithm are necessary[9]. However, noise can affect the EMD method's accuracy, so an adaptive filtering technique is suggested to improve the denoising process[10][11]. The seasonal decomposition approach can also be used to understand trends in time series. An integrated EMD adaptive threshold denoising approach (IEMD-ATD) is used, and it performs better than other denoising methods in reducing high-frequency noise from a noisy signal[12]. The researchers plan to use enhanced EMD algorithms and new thresholding strategies to further improve denoising performance in future studies. They have developed a noise reduction method based on enhanced EMD and forward linear prediction (FLP) to break down outputs into intrinsic mode functions (IMFs), and manipulate them to select noise-only IMFs, mixed IMFs, and residual IMFs[13]. They have combined enhanced EMD and FLP in an alternate noise-assisted EMD method for reducing noise in outputs.

2.2 SUMMARY

This chapter provides an overview of previous research related to the temperature drift of tuning fork gyroscopes. It summarizes the contributions made in this field, including the use of nonlinear prediction models and machine learning algorithms that utilize higher order spaces as input to solve nonlinear problems. The next chapter will focus on tuning fork gyroscopes, which detect changes in orientation through the Coriolis effect. It will discuss various methods, including neural networks, that have been used in earlier studies to compensate for bias. The following chapter will provide a description of the system being studied.

Chapter 3

SYSTEM DESCRIPTION

3.1 Overview

In this chapter, a detailed exploration of the tuning fork gyroscope is presented. Over the course of more than a century, extensive research, experimentation, and advancements in navigation technology have led to the creation of the tuning fork gyroscope. This device is crucial for ensuring flight safety, reducing human error, and achieving precision in both manned and unmanned aerial vehicles. The device works on the principle of the coriolis effect theory, which generates a signal representing the system's rate of rotation by measuring the deviation of the tuning fork from its oscillation plane. The tuning fork is also utilized for assessing vibratory hearing and sensation as it produces vibrations at a specific frequency when struck on the heel of a hand.

3.2 Tuning Fork Gyroscope

Tuning fork gyroscopes are based on the physics concept that an object in motion tends to remain in motion in the same plane as its support, and are also known as "Coriolis vibratory gyroscopes" due to their reliance on the Coriolis effect. The Coriolis force causes the perpendicular deflection of a moving object due to rotation, and serves as the coupling agent between the two resonant working modes in the TFG, which can be thought of as a coupled resonator system. The devices' dynamics are governed by Newton's second law of motion. The drive mode in these devices is typically a one-degree-of-freedom resonator that functions as a spring-mass damper system consisting of a proof mass, a drive mode suspension system, and a drive

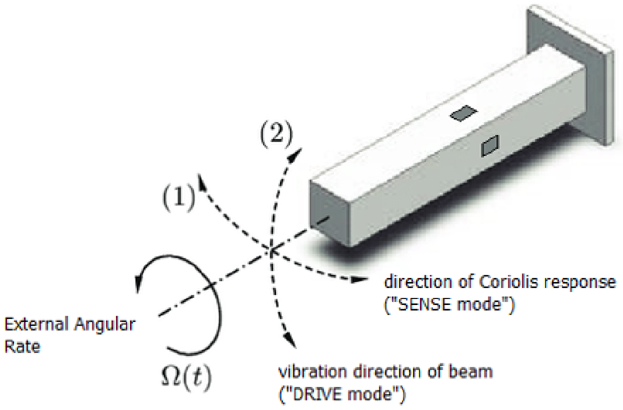

Figure 3.1: Schematic Diagram of Tuning Fork gyroscope

damping made up of viscous and thermoelastic damping. Tuning fork gyro sensors, which are often supported in a flat manner, are widely used to detect rotation in various applications, such as vibration prevention in cameras and automobile navigation systems. In recent years, the use of flatly supported tuning fork vibratory gyro sensors for vehicle control applications has been studied. In such applications, sensors need to be highly precise and possess strong vibration and shock resistance as they can have a significant impact on the safety of vehicles.

3.2.1 Coriolis Effect

The Coriolis force was historically approached using coordinate transformation techniques, which did not clarify its physical significance in atmospheric processes and simple mechanical systems. Instead, studying Coriolis's scientific career and achievements demonstrates that the force's discovery was linked to advancements in early 19th-century mechanical and industrial processes, rather than earth sciences. The conservation of angular momentum only holds true when there is no torque present around the vertical axis.

The Coriolis effect causes moving objects to deflect when motion is represented in a rotating reference frame. The deflection direction depends on the direction of rotation. Newton's law of motion describes an object's motion in a non-accelerating frame of reference. When Newton's laws are applied to a uniformly rotating frame of reference, the Coriolis and centrifugal forces emerge, and their magnitude is proportional to both forces. The Coriolis force is proportional to the object's speed in the rotating frame and acts perpendicularly to both the body's velocity and the rotation axis, while the centrifugal force is proportional to the separation of the body from the spinning frame's axis and acts radially outward. These additional forces are called inertial forces, fake forces, or pseudo forces, and they allow the use of Newton's law in rotating systems.

3.2.2 Coriolis Effect on Gyros

If an external torque is applied to a rotating gyroscope perpendicular to its spin axis, the velocity of the gyroscope's rim changes direction rapidly in relation to the external torque axis. As a result, the Coriolis force acting on the rim causes the gyroscope to tilt at a right angle to the direction it would have tilted due to the external torque. This characteristic leads to the stable alignment of spinning bodies in space.

3.2.3 Working Of Tuning Fork Gyro

The rate of rotation of a system is detected through the measurement of the tuning forks' displacement from their plane of oscillation. In a MEMS device, a rate gyroscope is formed by two tuning forks made of piezoelectric materials, with quartz being commonly used. The resonant modes of the tuning forks are utilized in the piezoelectric rate gyroscope to generate the measuring signal for detecting the system's rotational motion and angular velocity.
Two resonant modes are used:

1.Drive mode

2.Sense mode

The two modes of operation in a gyroscope function as the driving and sensing mechanisms. In the drive mode, electrodes are placed on the drive tines' surfaces, creating an electric field that drives the tuning fork at its resonance frequency in the xy-plane.In contrast to the driving mode, the sense mode induces vibration of the sense tines in a direction perpendicular to the tuning fork plane, specifically along the z-axis. This out-of-plane sense mode motion is produced by the Coriolis force when the gyroscope rotates around the y-axis, which can be detected directly via the piezoelectric effect. However, the in-plane movement is sensed through a different mechanism.

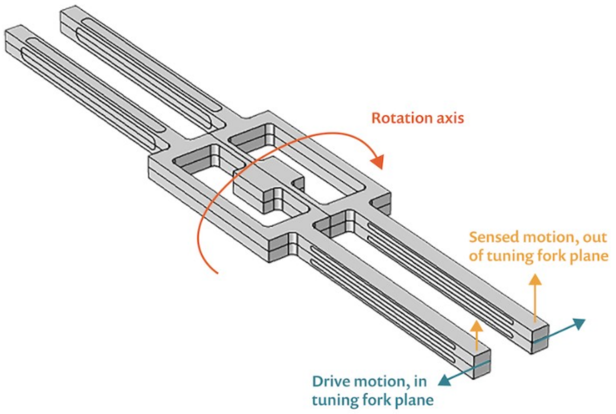

Figure 3.2: Tuning Fork gyroscope

The various components work together to assist the system in detecting and correcting any imbalanced or tilted orientation, which is crucial for safety and preventing damage in some mechanical systems, as well as maintaining proper orientation in others. MEMS gyroscopes are utilized in skid control systems and rollover detection due to their ability to maintain balance.

1. Driving Mode:

Beneath each vibration mass block of the gyroscope, there are two differential drive electrodes and a detection electrode. The application of voltage to the differential drive electrode plates results in the generation of an electrostatic force that drives the block to oscillate horizontally by bending the vibration beam. However, because the azimuth angle of the vibration beam is less than 90 degrees, it also generates a vertical driving motion component. Therefore, in the driving mode, the vibration mass block shows a three-dimensional vibration motion that includes a reciprocating motion frequency in the horizontal direction and a driving component motion in the vertical direction.

2. Detection Mode:

The gyroscope's driving mode involves applying voltages to differential drive electrode plates, which generate an electrostatic force causing horizontal oscillation of the vibration mass block. However, because the angle of the vibration beam is less than 90 degrees, a vertical driving motion component is also produced. This results in three-dimensional vibration motion comprising the same frequency reciprocating motion in the horizontal direction and a driving component motion in the vertical direction[14].

When the gyroscope is in driving mode and there is angular velocity input on the sensitive axis, the Coriolis force is generated in the detection direction following the Coriolis force principle. This force leads to torsional deformation of the vibration beam, causing the vibration mass block to move up and down in the vertical direction.

The tuning fork can be used to test hearing and vibratory sensation by striking it against a surface such as the hand or a table (air conduction and bone conduction). When holding the tuning fork, it is advisable to grip it by the stem rather than the prongs.

3.3 Advantages

- Designed with a symmetrical structure.
- Differential mode of operation common mode errors are cancelled.
- Doubles the amplitude of the output signal.
- High sense capacitance.

3.4 Disadvantages

- Small displacement in the sense mode.
- Large zero bias errors caused by the slight misalignment of the mass centres of the individual .

3.5 SUMMARY

This chapter provides a comprehensive discussion on the tuning fork gyroscope, including its construction, working principle, and operation. The following chapter will focus on the methodology used in the thesis.

Chapter 4

METHODOLOGY

4.1 Overview

This chapter focuses on the bias compensating method for the tuning fork gyroscope, which involves designing and implementing an AI-based compensation technique to address bias drift in the sensor. Through analysis of sensor drift data and testing of multiple AI models, this technique can effectively compensate for changes in different environmental conditions. Time series decomposition methods such as Seasonal Decomposition and EMD are utilized for denoising purposes. Ultimately, a combination of seasonal decomposition and EMD with LSTM approach is recommended, and its performance is compared to that of a standalone LSTM.

The study aimed to analyze the performance of tuning fork gyroscopes (TFGs) under multiple thermal cycling conditions and develop bias compensation techniques based on AI models. Five thermal cycling datasets, including Amplitude, Frequency, Quadrature, and Rate, were used at different temperature conditions. The correlations between variables in the datasets were identified and measured using various methods. To denoise the input data, time series approaches such as Seasonal Decomposition and Empirical Mode Decomposition (EMD) were employed. The denoised data was then inputted to Long Short-Term Memory (LSTM) to obtain the compensated output, and the results were compared with those of a single LSTM model.

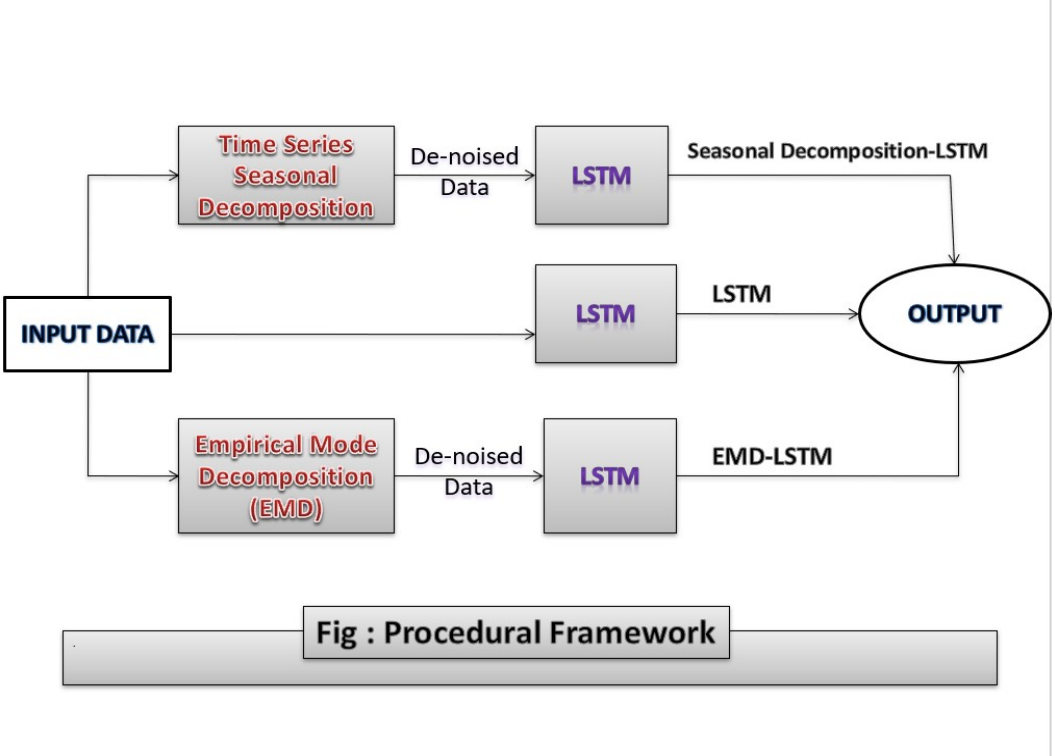

Figure 4.1: Procedural Framework

4.2 Correlation

Correlation is a statistical measure of the strength and direction of the linear relationship between two variables. It helps to understand how strongly two variables are related and to what extent they are related. A high correlation indicates a strong relationship between variables, while a low correlation indicates a weak relationship. Understanding correlations between variables is important in data analysis and modeling. Correlation can be positive or negative, indicating whether the variables change in the same direction or in opposite directions. A zero or neutral correlation indicates no relationship between the variables. In a positive correlation, when one variable increases, the other variable also tends to increase, and vice versa. In a negative correlation, when one variable increases, the other variable tends to decrease, and vice versa.

4.2.1 Pearson Correlation

The Pearson correlation coefficient is used to measure the strength of the linear relationship between two continuous variables, especially when they are normally distributed. It is a widely used indicator for identifying linear correlations, and it is calculated using a least-squares fit. A value of 1 indicates a perfect positive relationship, -1 indicates a perfect negative relationship, and 0 indicates no correlation between the variables. The Pearson correlation coefficient is also known as "correlation coefficient."

$$r = \frac{\sum_{i=1}^{n}(x_i - \overline{x})(y_i - \overline{y})}{\sqrt{\sum_{i=1}^{n}(x_i - \overline{x})^2 \sum_{i=1}^{n}(y_i - \overline{y})^2}} \tag{4.1}$$

where ,

n=quantity of information

$\sum(x) = Total of the first variable value.$

$\sum(y) = Total of the second variable value.$

$\sum(xy) = sum of the product of first and second variable$

$\sum(x^2) = sum of the squares of first value$

$\sum(y^2) = sum of the squares of second value$

4.2.2 Spearman correlation

The Spearman correlation is a statistical test that measures the degree of association between two ordinal variables, and it assesses the monotonic relationship between them. This test is appropriate for variables that are not normally distributed and have a non-linear relationship. The Spearman correlation coefficient, also known as rho, is similar to the Pearson correlation coefficient, but it is a rank-based measure that is useful in analyses of ordinal qualities. Unlike Pearson's correlation coefficient, which can only be used with continuous data, Spearman's rho can be used with any type of data.

$$\rho = 1 - \frac{6\sum d_i^2}{n(n^2-1)} \tag{4.2}$$

where,

n= no. of observation

di=difference between observation

$\rho = spearman's rank coefficient.$

4.2.3 Kendall correlation

Kendall's tau is a measure of the strength of a monotonic relationship between two variables, similar to Pearson's correlation coefficient. It is also suitable for non-normally distributed data, just like Spearman's rho. Kendall tau can be computed for both ordinal and continuous data. However, Kendall's tau differs from Spearman's rho in that it assigns a greater penalty for non-consecutive (in terms of the ranked variables) differences. Kendall's tau for the sample is calculated as the number of concordant pairs minus the number of discordant pairs.

$$\tau = \frac{c-d}{c+d} = \frac{S}{\begin{pmatrix} n \\ 2 \end{pmatrix}} = \frac{2S}{n(n-1)} \tag{4.3}$$

where,c = the number of concordant pairs and d = the number of discordant pairs

4.3 Time Series Seasonal Decomposition

Seasonal Decomposition is a useful method for analyzing and understanding time series data by breaking it down into its components of level, trend, seasonality, and noise. This is especially helpful in dealing with the complexities and noise of real-world time series data, where both additive and multiplicative effects can occur, and trends and seasonality can vary. By separating time series data into systematic and non-systematic components, decomposition can aid in choosing appropriate forecasting methods. Decomposition is primarily used for time series analysis and can guide the creation of forecasting models by providing a structured approach to handling the various components of time series data.[15].

- **Systematic:** Time series elements with consistency or recurrence that may be described and modelled.

- **Non-Systematic:** Time series elements that can't be accurately modelled.

Level, trend, and seasonality are considered to be the three systematic components of a given time series, whereas noise is considered to be the non-systematic component.
Level: The series average value.
Trend: The value's upward or downward movement over time.
Seasonality: The series recurring short-term cycle.
Noise: The series random variation.

A series is considered to be an amalgamation or combination of these four elements.A level and noise exist in every series. It's optional to include the trend and seasonality components.The components can be thought of as mixing either additively or multiplicatively, which is useful[16].

4.3.1 Additive Model

According to an additive model, the components should be added as follows:

$$y(t) = Level + Trend + Seasonality + Noise \tag{4.4}$$

When modifications are continuously made by the same amount across time, a linear additive model is present. A straight line represents a linear tendency. A linear seasonality has a constant frequency (cycle width) and magnitude(height of cycles).Here we uses additive model.

4.3.2 Multiplicative Model

$$y(t) = Level * Trend * Seasonality * Noise \tag{4.5}$$

Nonlinear models like quadratic or exponential are examples of multiplicative models. With time, changes can get bigger or smaller. A curving line indicates a nonlinear trend. A nonlinear seasonality changes in frequency and/or amplitude over time, either more frequently or less frequently.

4.4 Empirical Mode Decomposition(EMD)

Conventional signal processing techniques are not effective for analysing non-linear and non-stationary signals as they are incapable of capturing their characteristics precisely. To overcome this limitation, time-frequency analysis methods are employed to examine the frequency domain characteristics of the signal at different time intervals. Empirical Mode Decomposition (EMD) is a typical nonlinear non-stationary algorithm that adapts its time-frequency resolution to the signal, making it useful in various applications, such as medical denoising, due to its enhanced resolution[4].

Huang et al. developed the Empirical Mode Decomposition (EMD) technique in 1998 to analyze non-stationary and non-linear signals.EMD stands for Empirical Mode Decomposition, which is a technique used for analyzing signals that are non-linear and non-stationary. This method breaks down the data into a finite number of unique components called Intrinsic Mode Functions (IMFs), which are dependent on the local characteristic time scale of the data[3]. Each Intrinsic Mode Function (IMF) is a sequence of signals with a distinct oscillation mode that can represent specific physical meanings of the original signal. However, it must satisfy the following two requirements:

- In the entire data set, the number of extrema and the number of zero crossings must be identical or differ by no more than one.
- The average value of both the envelope obtained from the local maxima and the envelope derived from the local minima is always zero.

4.4.1 EMD Standard Alogirthm

The EMD algorithm is a data-driven approach that can decompose any signal into a set of Intrinsic Mode Functions (IMFs) and a residual component. The algorithm adapts to the characteristics of the signal and extracts the IMFs based on the local time scales of the data. Figure 4.2 illustrates the steps of the screening process used to obtain the IMFs and residual component[12].

EMD is in fact a sifting process. The EMD algorithm is described as follows:

Step 1: Identify all the points in the original data x(t) where there are local minimums and maximums, such as the minimum value at time t (min(t)) and the maximum value at time t (max(t)).

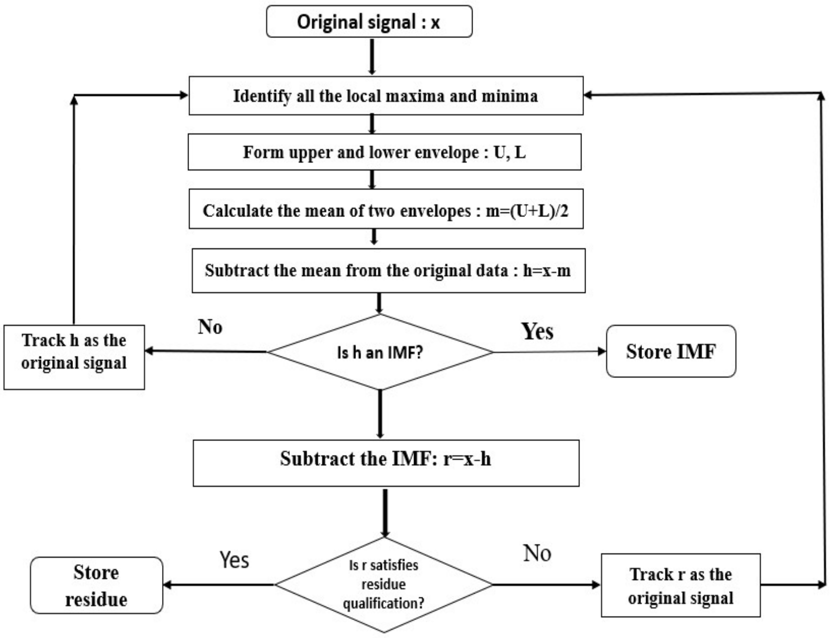

Figure 4.2: Flowchart of the precise EMD screening steps

Step 2: Use cubic spline interpolation to compute the maximum envelope, e(t)max, and minimum envelope, e(t)min, based on the local maxima and minima identified in the previous step.

Step 3: Determine the average $\mathrm{m}_1(t)$ of $\mathrm{e}_{\max}(t)$ and $e_{\min}(t)$:

$$\mathrm{m}_1(\mathrm{t}) = \frac{(\mathrm{e}_{\max}(\mathrm{t}) + \mathrm{e}_{\min}(\mathrm{t}))}{2}$$

Step 4: The first intrinsic mode function $\mathrm{h}_1(\mathrm{t})$ is given as:

$$\mathrm{h}_1(\mathrm{t}) = \mathrm{x}(\mathrm{t}) - \mathrm{m}_1(\mathrm{t})$$

Step 5: Verify that the two requirements are met by $h_1(t)$. In that case, residue $r_1(t)$ is used in place of the raw data x, and $h_1(\mathrm{t})$ is labelled as the first IMF of x(t).

$$r_1(t) = x(t) - h_1(t)$$

Otherwise, replace the raw data $x(t)$ with $h_1(t)$.

Step 6: Repeat the previous steps until the residue satisfies certain conditions such as being a monotonic function, a constant value, or a function with a single extremum. This indicates that no more IMF can be extracted and the sifting process is completed.The original data can be represented as a sum of the extracted IMFs and the final residue.

$$\mathrm{x(t)} = \sum_{\mathrm{i=1}}^{\mathrm{n}} \mathrm{c_i(t)} + \mathrm{r(t)}$$

where $\mathrm{c_1(t), c_2(t), \ldots, c_n(t)}$ are the 1 th, 2th, ..., nth IMF, respectively, of the original data $\mathrm{x(t)}$, and the final residue $r(t)$ represents a trend of the original data.

4.5 Long Short-Term Memory (LSTM)

LSTMs are a type of RNN that can retain information over long time periods, enabling them to learn long-term dependencies. Recurrent neural networks (RNNs) contain neural network modules that repeat, but long short-term memory (LSTM) networks utilize gates, including the forget gate, input gate, and output gate, to selectively remember or forget information. The motivation for creating the LSTM network was to address the issue of vanishing gradients. As seen in Figure 4.3, the LSTM includes a memory block that is not present in traditional RNNs. LSTMs have a straightforward design with a repeating module that consists of a single tanh layer. While LSTMs also have a chain-like structure, the repeating module has a different structure compared to conventional RNNs.

Forget Gate(f): It determines to what extent to forget the previous data.

Input Gate(i): It determines the extent of information be written onto the Internal Cell State.

Output Gate(o): It determines what output(next Hidden State) to generate from the current Internal Cell State.

These are the three steps involved in designing the LSTM architecture:

Step 1: Determine the amount of previous data that the LSTM should store and remember for making predictions.

Step 2: Determine the contribution of the current input to the current state of the LSTM.

Step 3: Determine which part of the current state should be used to generate the output.

Step 1:

In the LSTM, the first step involves deciding which information should be kept or discarded

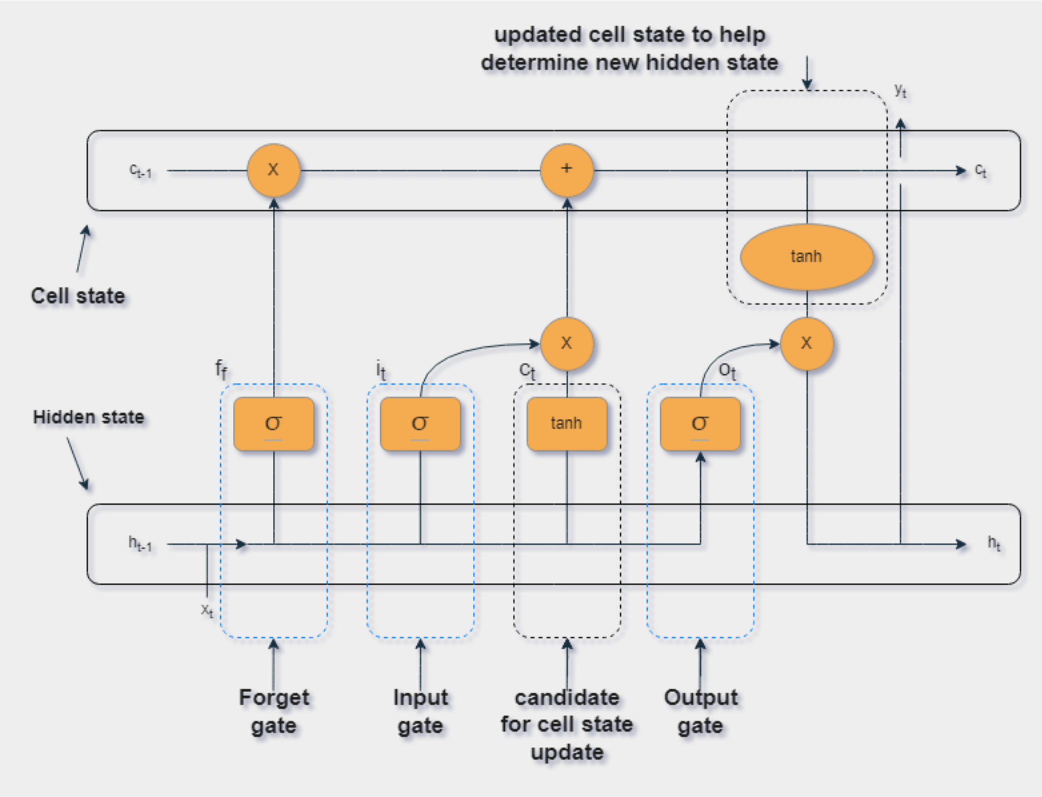

Figure 4.3: LSTM

from the cell state in the current time step. This decision is made by the forget gate, which uses a sigmoid function to determine which information should be omitted. The sigmoid function takes as input the previous state (ht-1) and the current input xt, and computes a value between 0 and 1 for each element of the cell state, where 0 means "completely forget this information" and 1 means "completely remember this information"[2].

$$f_t = \sigma\left(W_f \cdot [h_{t-1}, x_t] + b_f\right)$$

where ft is the forget gate,decides which information to delete that is not important from previous time step.

Step 2:

In the second layer of LSTM, there are two main components: the input gate and the tanh layer. The input gate uses the sigmoid function to determine which values should be allowed to pass through (0 or 1), while the tanh layer assigns weights to the passed values to determine their level of importance (-1 to 1). Together, these two components analyze the relevant information in the current input (x(t)) and decide which parts of it should be retained and passed on to the next layer.

$$\mathrm{i_t} = \sigma\left(\mathrm{W_i} \cdot \left[\mathrm{h_{t-1}}, \mathrm{x_t}\right] + \mathrm{b_i}\right)$$

where it is the input gate,determines which information to let through based on its significance in the current time step.

Step 3:

The third step of the LSTM involves determining the output. To do this, we first apply a sigmoid function that decides which parts of the cell state should be included in the output. Next, we apply the hyperbolic tangent (tanh) function to the cell state to scale the values between -1 and 1. Finally, we multiply the output of the sigmoid gate with the output of the tanh function to obtain the final output.

Recurrent Neural Networks (RNNs) have a weakness in their short-term memory, which makes it difficult to remember earlier information when processing long sequences of data, such as paragraphs of text. Moreover, during back propagation, RNNs face the issue of the vanishing gradient problem. The gradients, which are used to update the network's weights during training, shrink as they propagate through time, resulting in small gradient values that do not contribute significantly to learning. This problem particularly affects the earlier layers in the network, which receive smaller gradient updates and thus stop learning. As a result, RNNs can forget information from earlier time steps in longer sequences, leading to a limited short-term memory.

The tanh activation function is used in neural networks to regulate the values that flow through the network. It ensures that the output of the neural network stays between -1 and 1, preventing values from exploding or becoming insignificant due to various math operations. The sigmoid function is also used in neural networks, especially in the gates of LSTMs. The sigmoid function squishes values between 0 and 1, which is helpful in updating or forgetting data. The forget gate in an LSTM decides what information to keep or throw away, based on the previous hidden state and the current input, which is passed through the sigmoid function. The input gate updates the cell state by passing the previous hidden state and current input through a sigmoid function, which decides which values will be updated. The hidden state and current input are also passed through the tanh function to regulate the network. The cell state is then calculated by pointwise multiplication with the forget vector and pointwise addition with the output from the input gate. The output gate determines the next hidden state, which carries information from previous inputs and is used for predictions. The previous hidden state and current input are passed through a sigmoid function, and the newly modified cell state is passed through the tanh function. The output is the hidden state, which is carried over to the next time step along with the new cell state.

4.6 SUMMARY

In this chapter, a methodology for bias compensation was presented in detail. The first step involved using three types of correlations to determine the strength of the quantities. Since the input data was noisy, denoising methods like Seasonal decomposition and Empirical mode decomposition were employed to enhance the system's performance. Finally, the trends obtained from these approaches were fed separately into LSTM to compare Seasonal decomposition-LSTM and EMD. The next chapter will focus on the results and discussions.

Chapter 5

RESULTS AND DISCUSSIONS

5.1 Overview

The analysis of TFGs' performance during five thermal cycling tests involved dividing the data into a training set and test set.In the second thermal cycle of TFG, the rate was utilized as the training set for the LSTM neural network to optimize the model's hyperparameters. The other four thermal cycles were treated as distinct test datasets to assess the effectiveness of the forecasting models. To ensure that the data is normalized within the range of (0, 1) for both the training and test sets, the MinMaxScaler function from the Sklearn Library in Python was employed. During the validation phase, the predicted values were rescaled to compare them to the actual values. The Keras Library in Python was used for the entire project, and Adam was the optimizer for the LSTM models. Performance measurements in the study included standard deviation before and after compensation, along with root mean square error (RMSE).

5.2 Visualisation of Input data

In this chapter, there are visual representations for analyzing the performance of multiple thermal cycles of the Tuning Fork Gyroscope (TFG). These visualizations include data on Amplitude, Rate, Frequency, and Quadrature. Figure 5.1(a) and 5.1(b) illustrate the data for the first thermal cycle of the TFG, with a time scale of 20ms and 100s, respectively. Similarly, figures 5.2(a) and 5.2(b), 5.3(a) and 5.3(b), 5.4(a) and 5.4(b), and 5.5(a) and 5.5(b) show the data for the second, third, fourth, and fifth thermal cycles of TFG in 20ms and 100s, respectively.

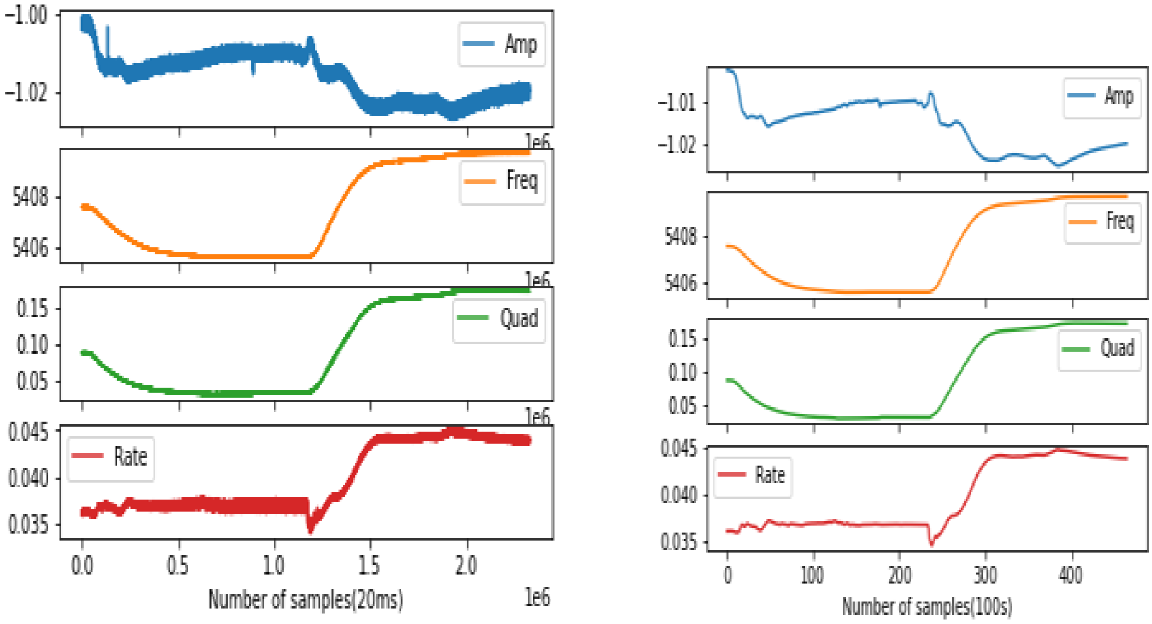

(a) First Thermal cycling data in 20ms

(b) First Thermal cycling data in 100s

Figure 5.1: First Thermal cycling data

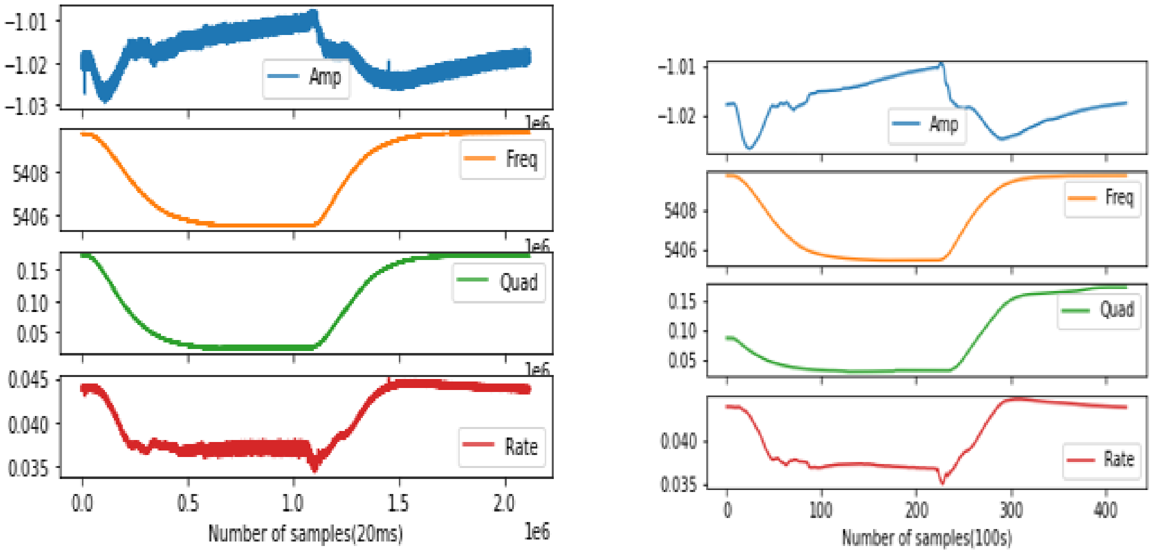

(a) Second Thermal cycling data in 20ms

(b) Second Thermal cycling data in 100s

Figure 5.2: Second Thermal cycling data

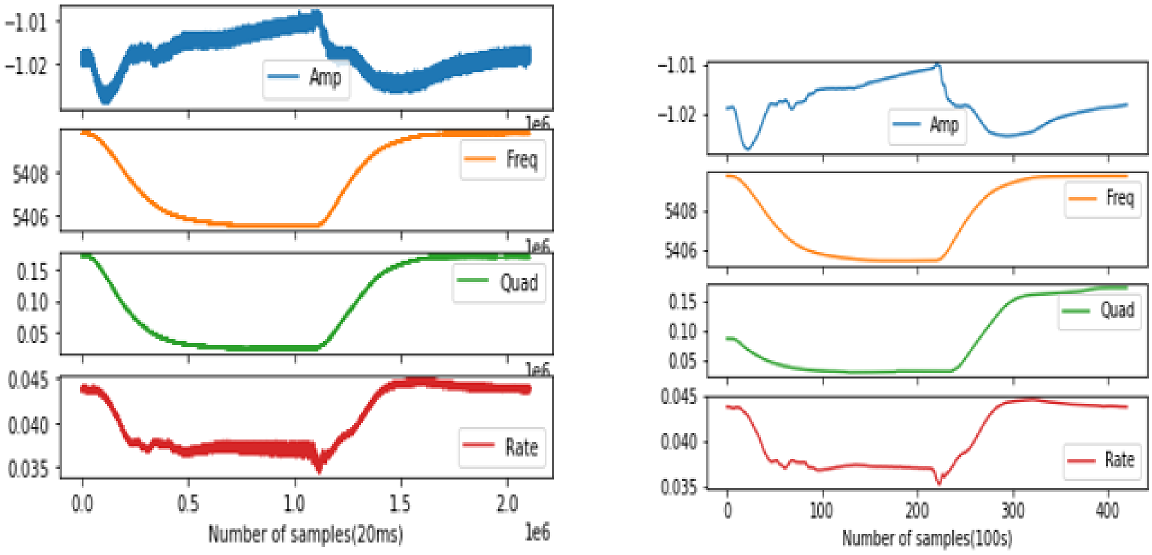

(a) Third Thermal cycling data in 20ms

(b) Third Thermal cycling data in 100s

Figure 5.3: Third Thermal cycling data

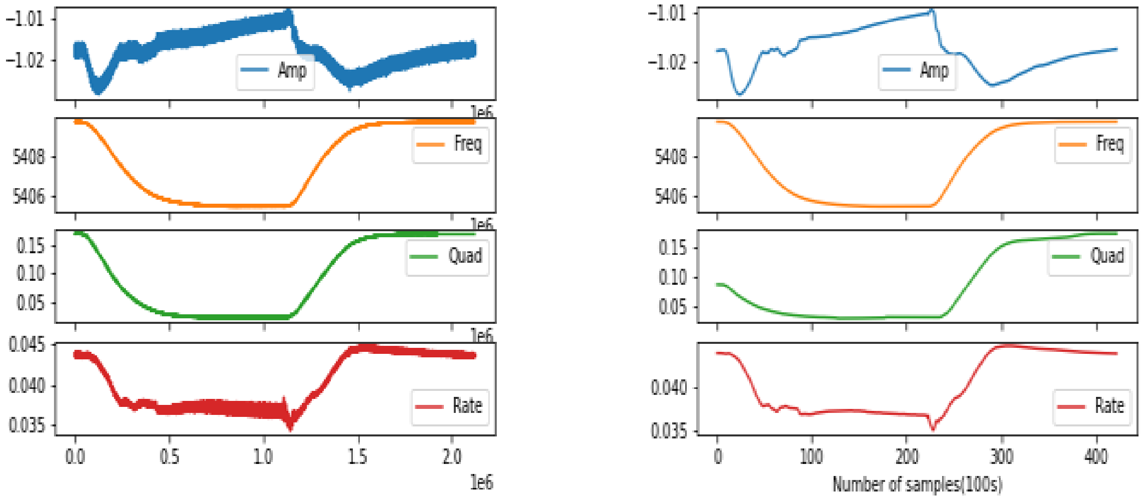

(a) Fourth Thermal cycling data in 20ms

(b) Fourth Thermal cycling data in 100s

Figure 5.4: Fourth Thermal cycling data

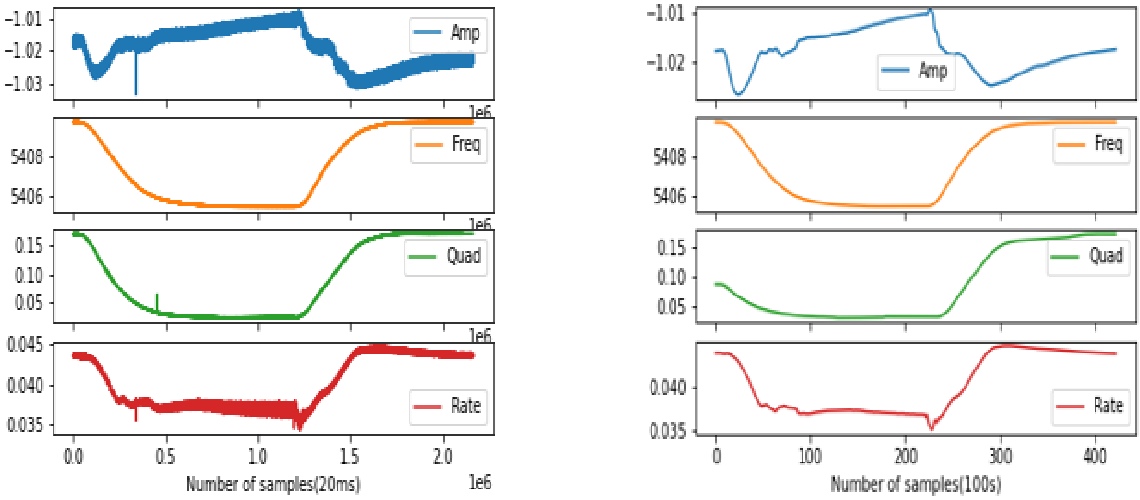

(a) Fifth Thermal cycling data in 20ms

(b) Fifth Thermal cycling data in 100s

Figure 5.5: Fifth Thermal cycling data

5.3 Correlation Results

5.3.1 Pearson Correlation

The figures 5.6(a), 5.6(b), 5.7(a), 5.7(b), and 5.8 illustrate the Pearson correlation among the Amplitude, Frequency, Quadrature, and Rate for the first, second, third, fourth, and fifth thermal cycles, respectively.

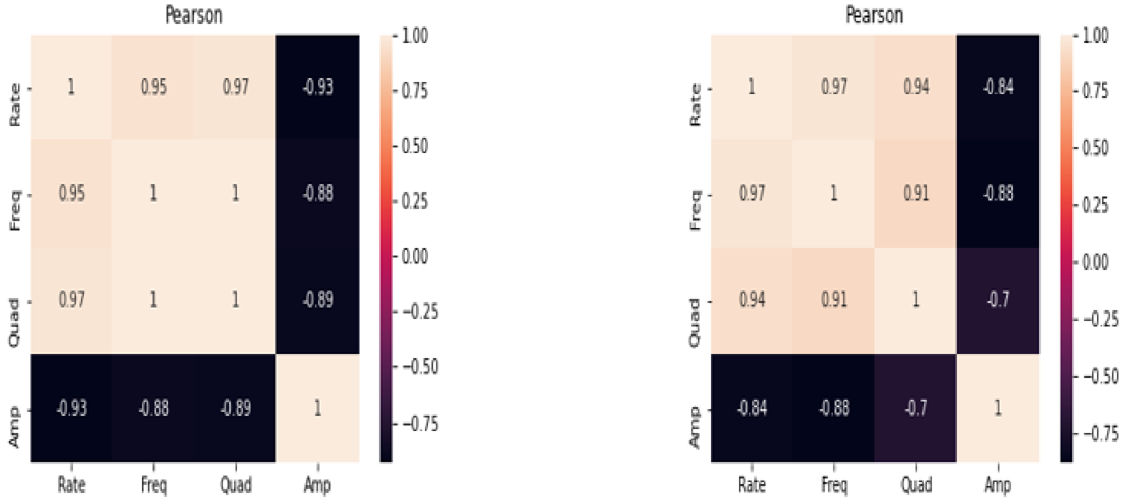

(a) Pearson correlation for first thermal cycle

(b) Pearson correlation for second thermal cycle

Figure 5.6: Pearson Correlation Results of first and second thermal cycles

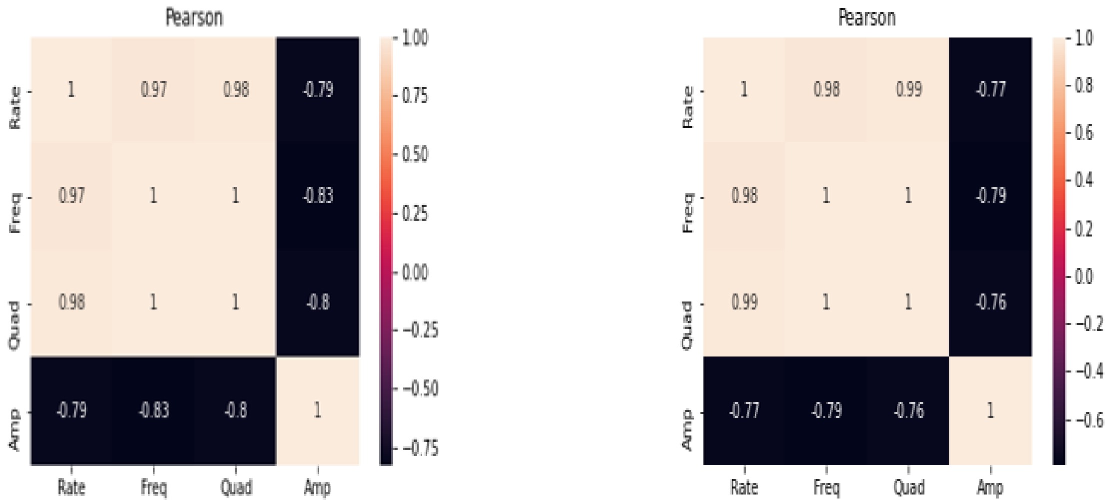

(a) Pearson correlation for third thermal cycle

(b) Pearson correlation for fourth thermal cycle

Figure 5.7: Pearson Correlation Results of third and fourth thermal cycles

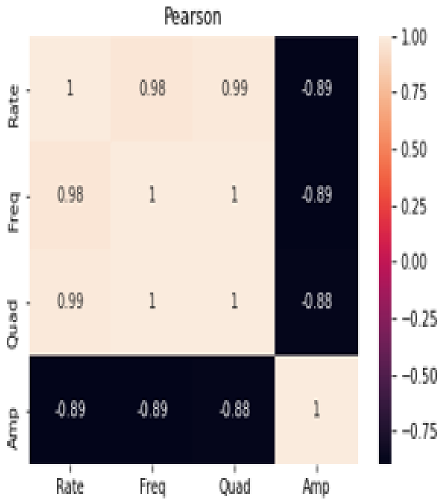

Figure 5.8: Pearson correlation for fifth thermal cycle

Table 5.1 shows Pearson Correlation results in multiple thermal cycling test data.It shows strong positive correlation in Rate vs Frequency and in Rate vs Quadrature. Strong negative correlation in Rate vs Amplitude in all thermal cycling tests. Pearson correlation is more suitable for the this work which shows more stronger correlations than the other two types of correlation.

Table 5.1: Pearson correlation results

SL.no	Data	Rate Vs Amplitude	Rate Vs Frequency	Rate Vs Quadrature
1	First thermal cycling test	Strong negative	Strong positive	Strong positive
2	Second thermal cycling test	Strong negative	Strong positive	Strong positive
3	Third thermal cycling test	Strong negative	Strong positive	Strong positive
4	Fourth thermal cycling test	Strong negative	Strong positive	Strong positive
5	Fifth thermal cycling test	Strong negative	Strong positive	Strong positive

5.3.2 Spearman Correlation

Figure 5.9(a), 5.9(b),5.10(a), 5.10(b),5.11 shows Spearman correlation between Amplitude, Frequency, Quadrature, Rate in first, second, third, fourth and fifth thermal cycles respectively. Table 5.2 shows Spearman Correlation shows strong positive correlation in Rate vs Frequency and in Rate vs Quadrature for the first two thermal cycling tests, moderate positive correlation for Rate vs Frequency and Quadrature in 3rd thermal cycling test and strong negative correlation in Rate vs Amplitude for three thermal cycling tests.

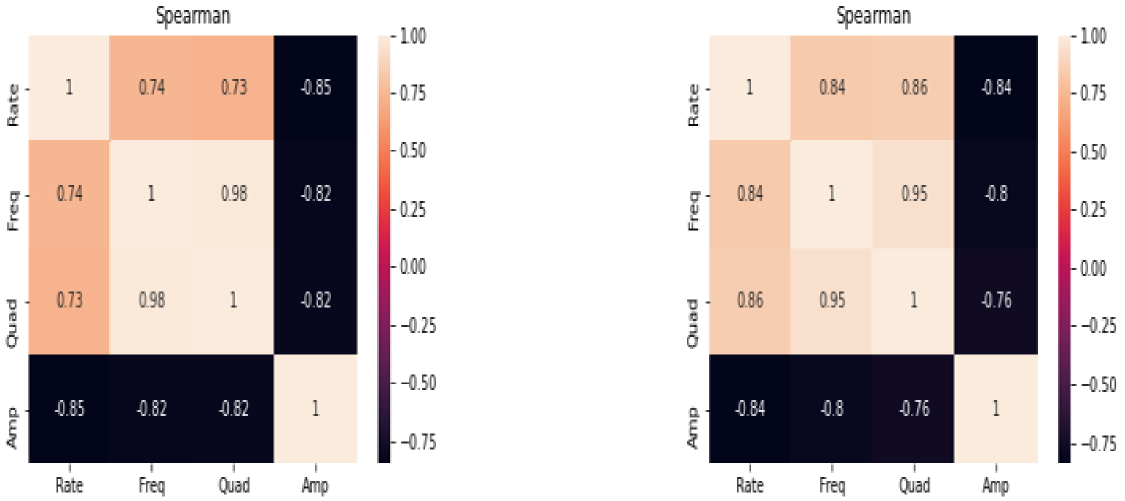

(a) Spearman correlation for first thermal cycle

(b) Spearman correlation for second thermal cycle

Figure 5.9: Spearman Correlation Results of first and second thermal cycles

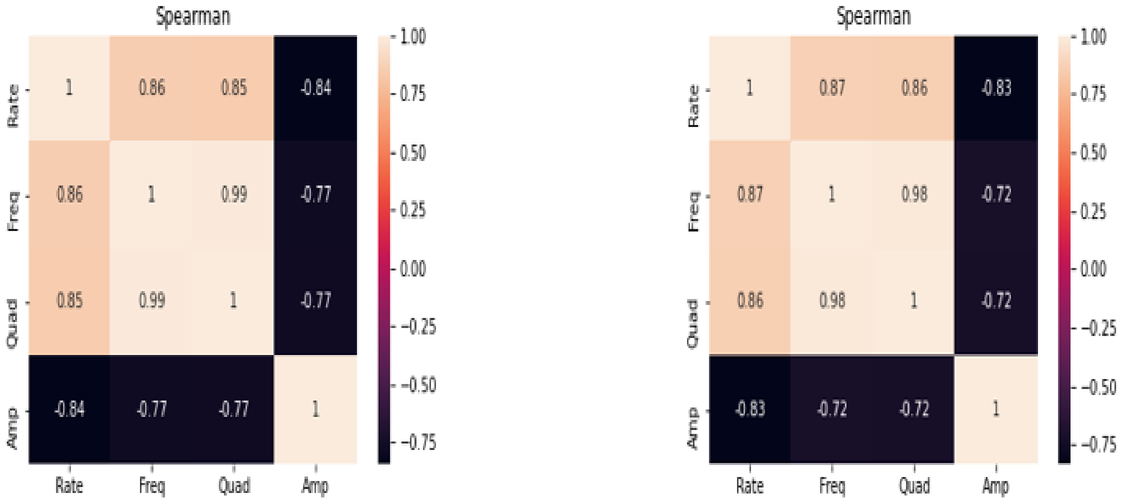

(a) Spearman correlation for third thermal cycle

(b) Spearman correlation for fourth thermal cycle

Figure 5.10: Spearman Correlation Results of third and fourth thermal cycles .

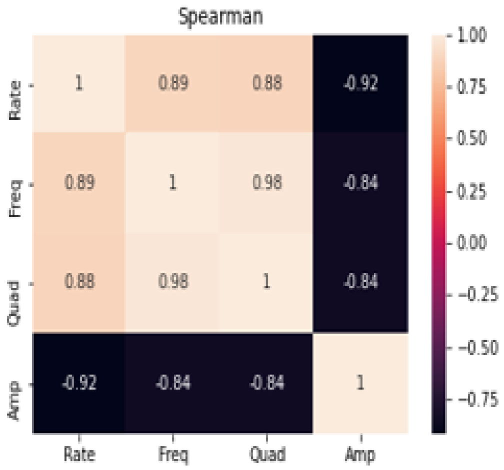

Figure 5.11: Spearman correlation for fifth thermal cycle

Table 5.2: Spearman correlation results

SL.no	Data	Rate Vs Amplitude	Rate Vs Frequency	Rate Vs Quadrature
1	First thermal cycling test	Strong negative	Strong positive	Strong positive
2	Second thermal cycling test	Strong negative	Strong positive	Strong positive
3	Third thermal cycling test	Moderate negative	Moderate positive	Moderate positive
4	Fourth thermal cycling test	Strong negative	Strong positive	Strong positive
5	Fifth thermal cycling test	Strong negative	Strong positive	Strong positive

5.4 kendall correlation

Figure 5.9(a), 5.9(b),5.10(a), 5.10(b),5.11 shows Spearman correlation between Amplitude, Frequency, Quadrature, Rate in first, second, third, fourth and fifth thermal cycles respectively. Table 5.2 shows Kendall Correlation shows moderate positive correlation in Rate vs Frequency and in Rate vs Quadrature. Moderate negative correlation in Rate vs Amplitude in three thermal cycling tests.

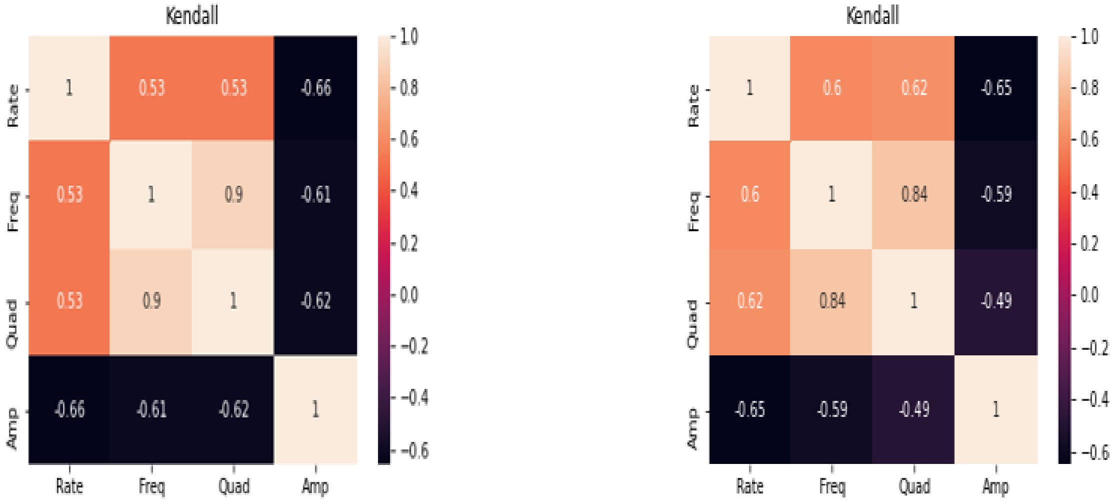

(a) kendall correlation for first thermal cycle

(b) kendall correlation for second thermal cycle

Figure 5.12: kendall Correlation Results of first and second thermal cycles

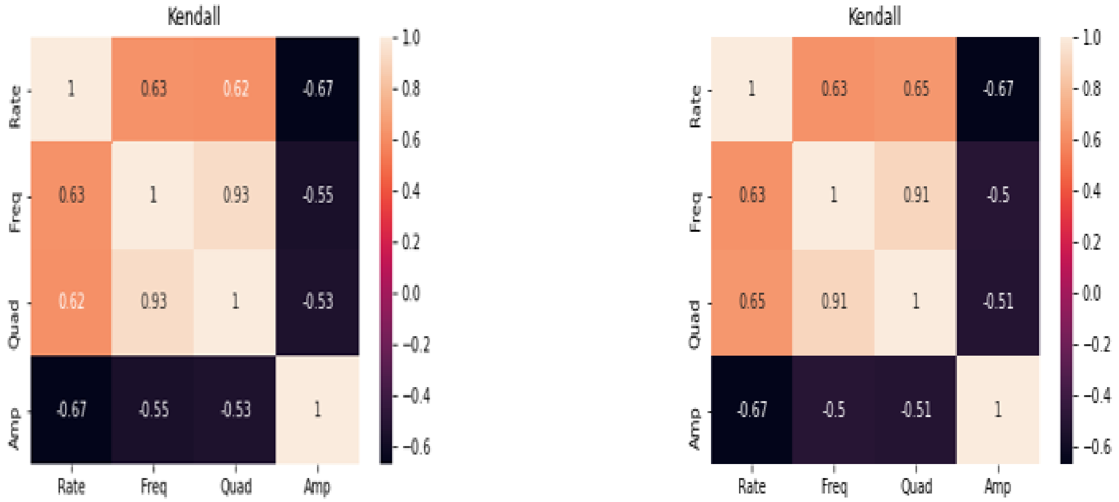

(a) kendall correlation for third thermal cycle

(b) kendall correlation for fourth thermal cycle

Figure 5.13: kendall Correlation Results of third and fourth thermal cycles .

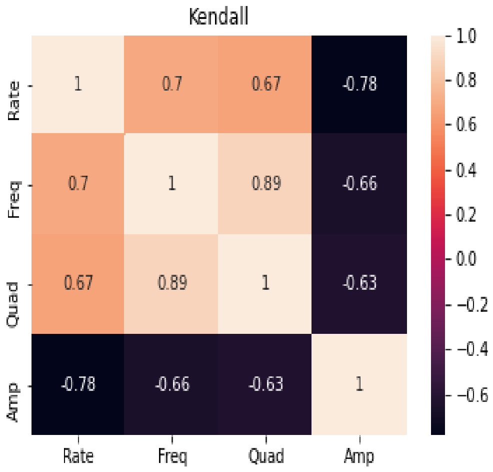

Figure 5.14: kendall correlation for fifth thermal cycle

Table 5.3: kendall correlation results

SL.no	Data	Rate Vs Amplitude	Rate Vs Frequency	Rate Vs Quadrature
1	First thermal cycling test	Moderate negative	Moderate positive	Moderate positive
2	Second thermal cycling test	Moderate negative	Moderate positive	Moderate positive
3	Third thermal cycling test	Moderate negative	Moderate positive	Moderate positive
4	Fourth thermal cycling test	Moderate negative	Moderate positive	Moderate positive
5	Fifth thermal cycling test	Moderate negative	Moderate positive	Moderate positive

5.5 LSTM Results

Figure 5.15(a)shows the graph of Actual rate Vs Predicted LSTM train data of second thermal cycle.Figure 5.15(b)shows the graph of Actual rate Vs Predicted LSTM test data of first thermal cycle. Figure 5.16(a),5.16(b) shows LSTM-Actual Rate Vs Predicted Rate of second (train data) and third (test data)thermal cycle. Figure 5.17(a),5.17(b) shows LSTM-Actual Rate Vs Predicted Rate of second (train data) and fourth (test data)thermal cycle.Figure 5.18(a),5.18(b) shows LSTM-Actual Rate Vs Predicted Rate of second (train data) and fifth (test data)thermal cycle.

The LSTM train data contains noise. To improve the system performance , denoising is vital . This denoising can be done with various methods such as Seasonal decomposition, EMD.

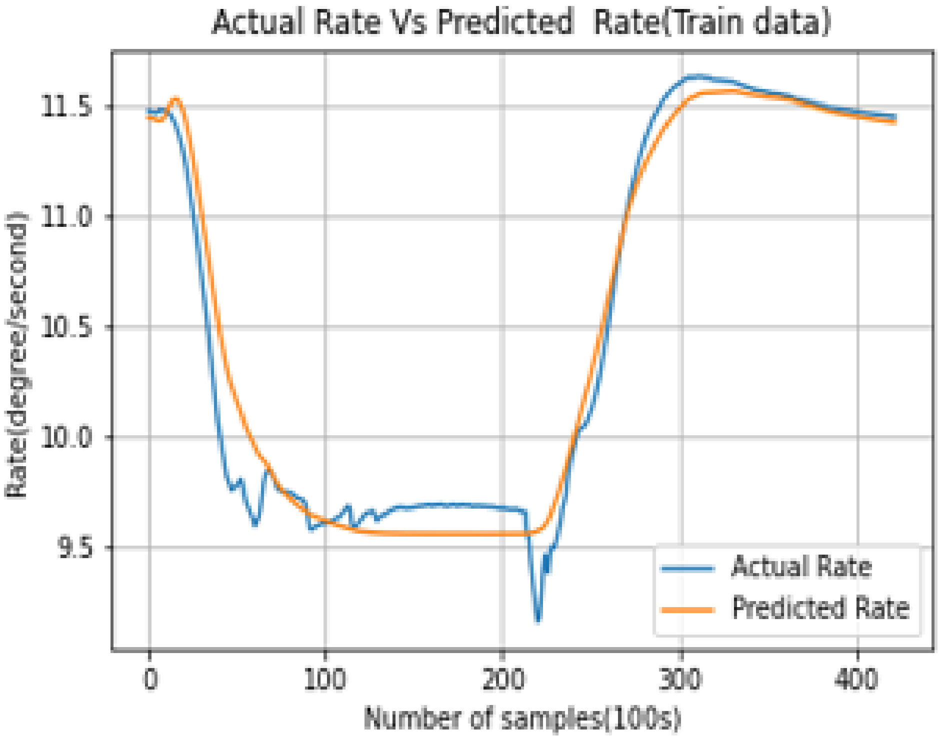

(a) Actual Rate Vs Predicted Rate(Train data)

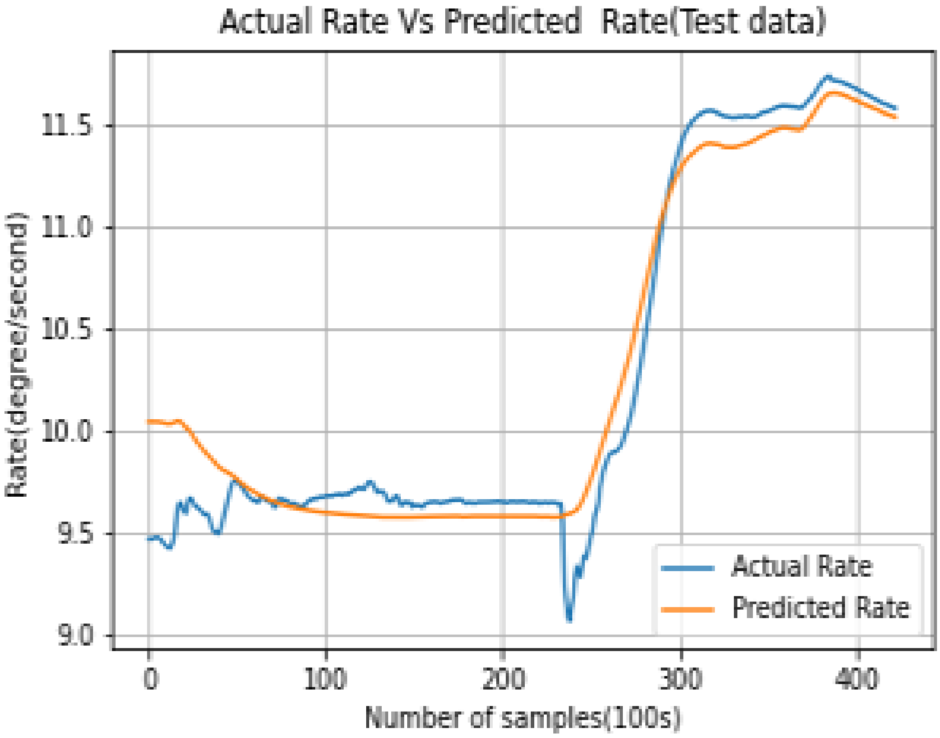

(b) Actual Rate Vs Predicted Rate(Test data)

Figure 5.15: LSTM-Actual Rate Vs Predicted Rate of second and first thermal cycle.

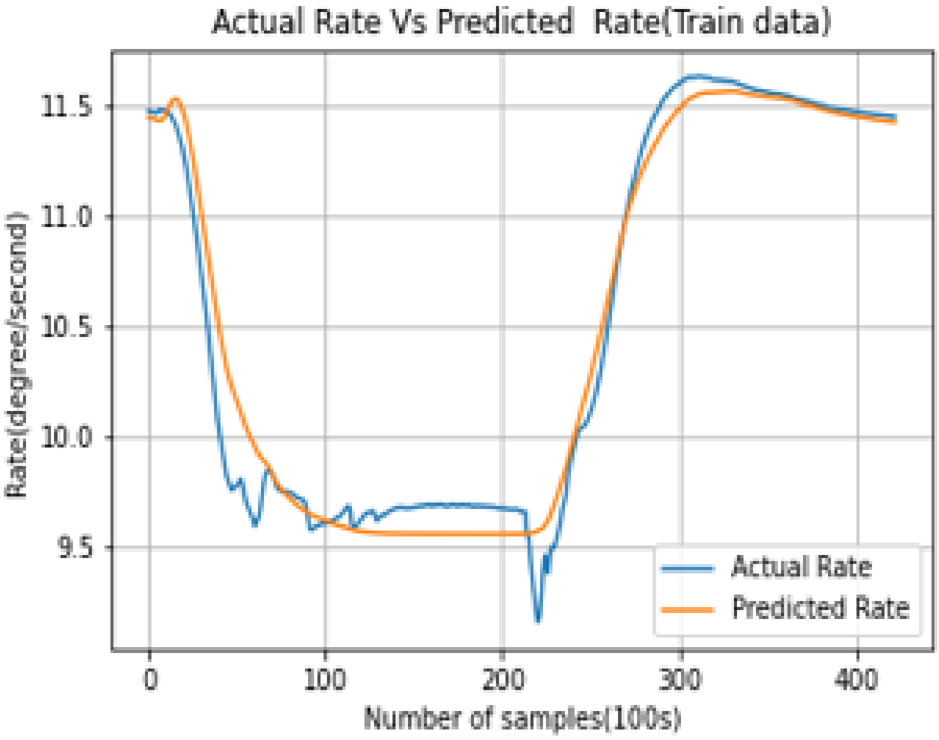

(a) Actual Rate Vs Predicted Rate(Train data)

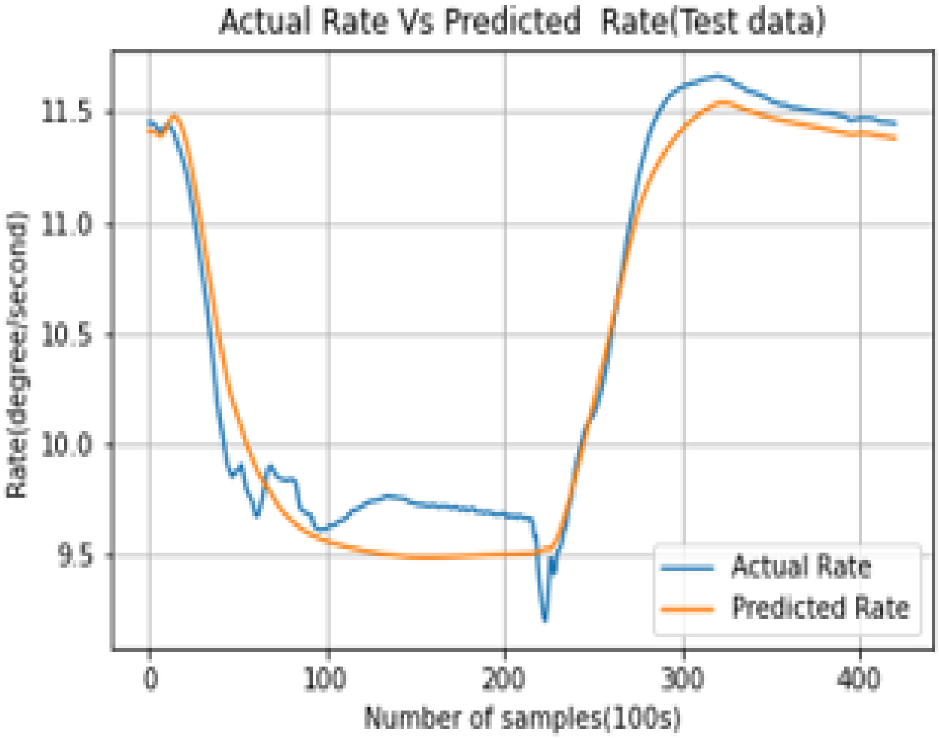

(b) Actual Rate Vs Predicted Rate(Test data)

Figure 5.16: LSTM-Actual Rate Vs Predicted Rate of second and third thermal cycle.

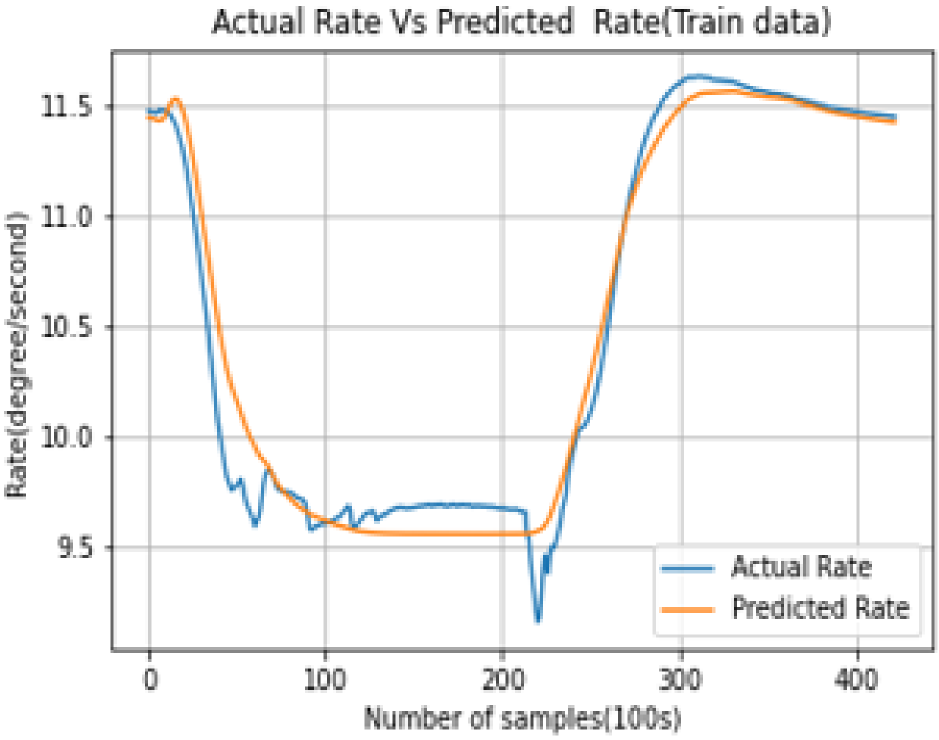

(a) Actual Rate Vs Predicted Rate(Train data)

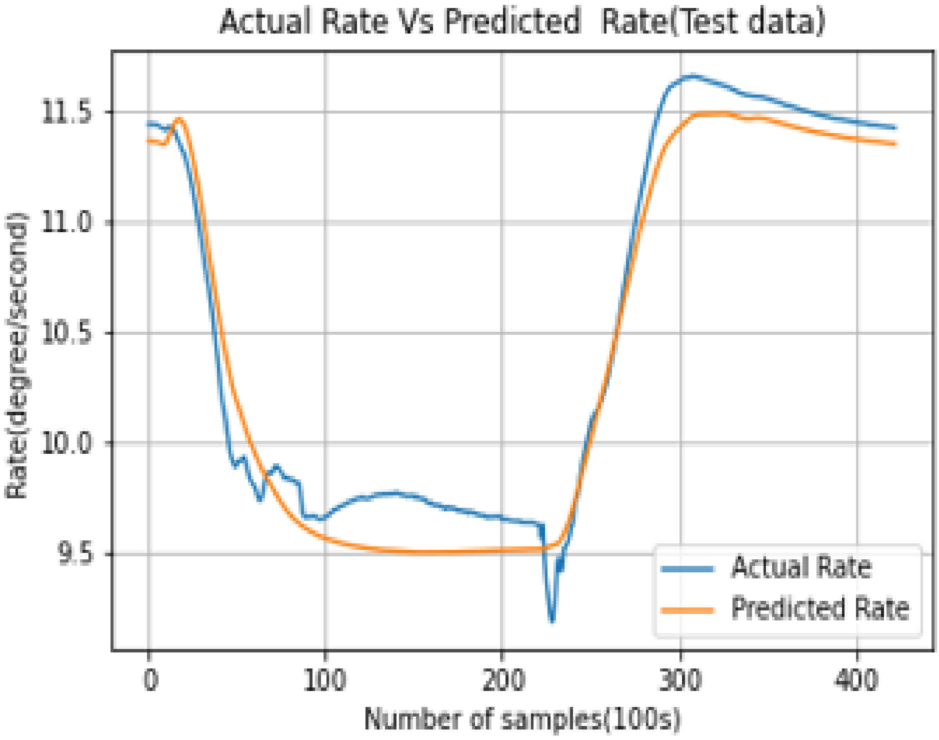

(b) Actual Rate Vs Predicted Rate(Test data)

Figure 5.17: LSTM-Actual Rate Vs Predicted Rate of second and fourth thermal cycle.

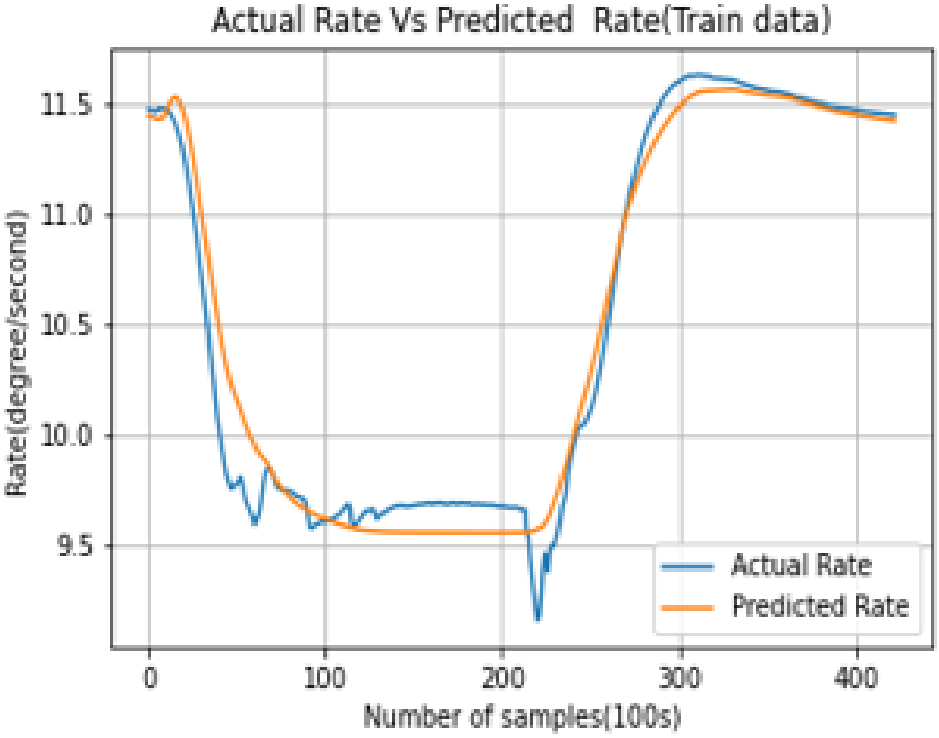

(a) Actual Rate Vs Predicted Rate(Train data)

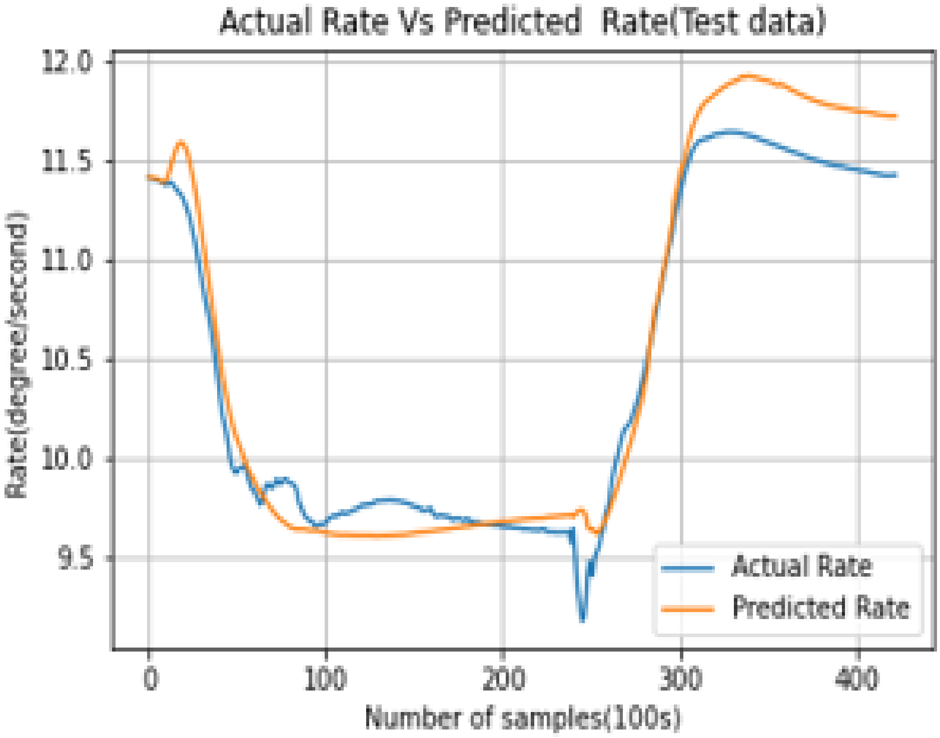

(b) Actual Rate Vs Predicted Rate(Test data)

Figure 5.18: LSTM-Actual Rate Vs Predicted Rate of first and fifth thermal cycle.

5.6 Seasonal Decomposition

It is a method used in time series analysis to represent a time series as sum of three components – a linear trend ,the periodic(seasonal) component and random residuals. It is useful in analysis of time series affected by factors that change in time in a cyclic(periodic)manner.

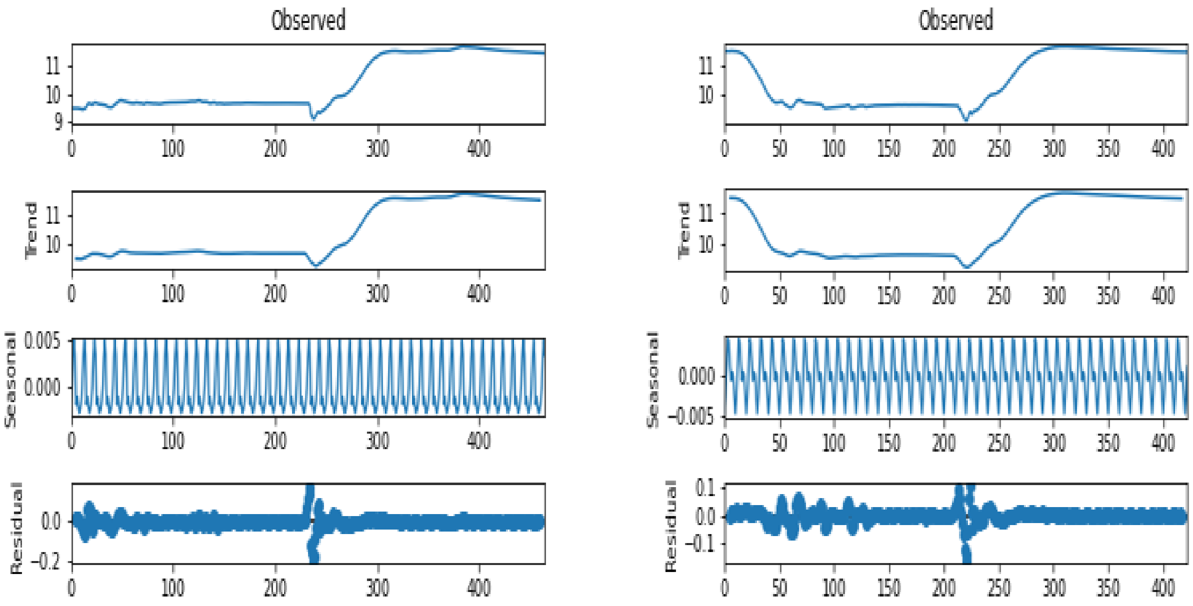

(a) Seasonal Decomposition of first Thermal cycle (b) Seasonal Decomposition of second Thermal cycle

Figure 5.19: Seasonal Decomposition of first and second thermal cycle.

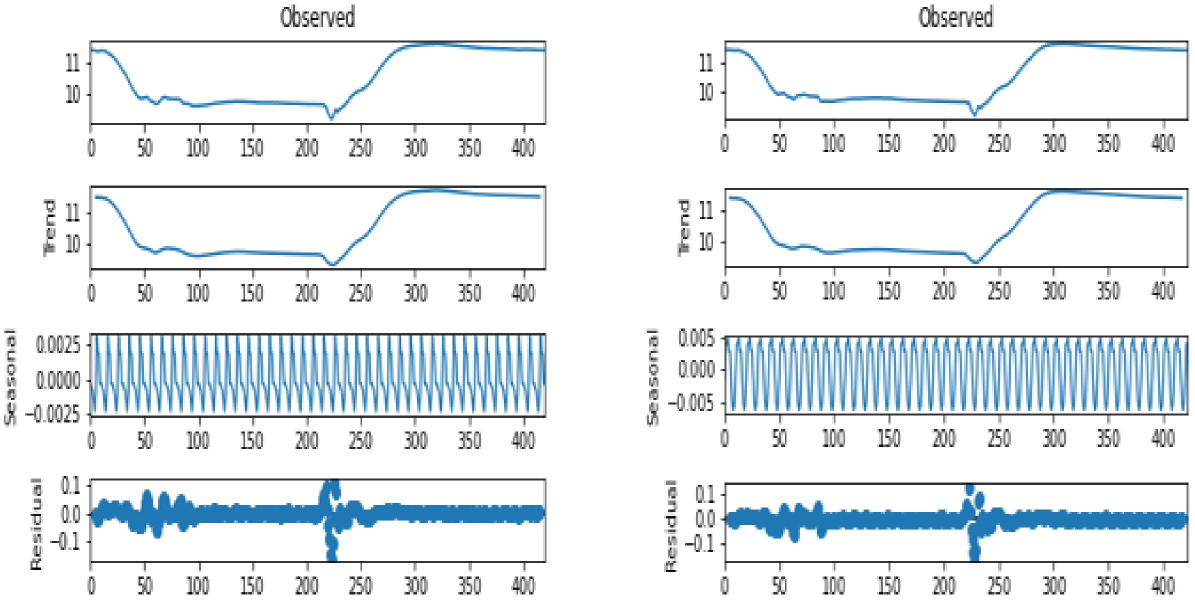

(a) Seasonal Decomposition of third Thermal cycle (b) Seasonal Decomposition of Fourth Thermal cycle

Figure 5.20: Seasonal Decomposition of third and fourth thermal cycle.

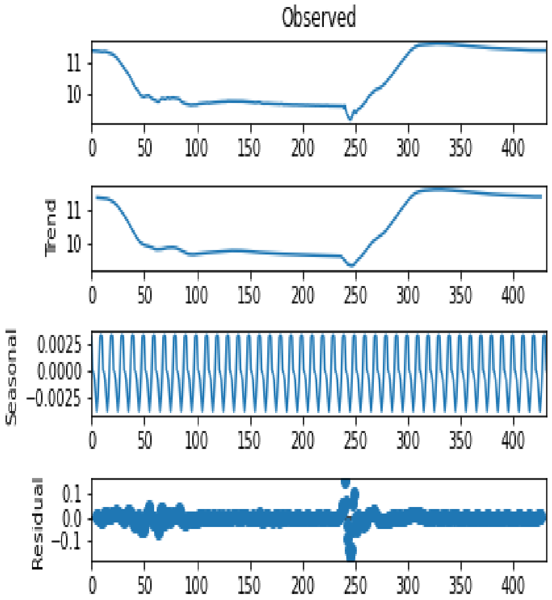

Figure 5.21: Seasonal Decomposition of fifth thermal cycle.

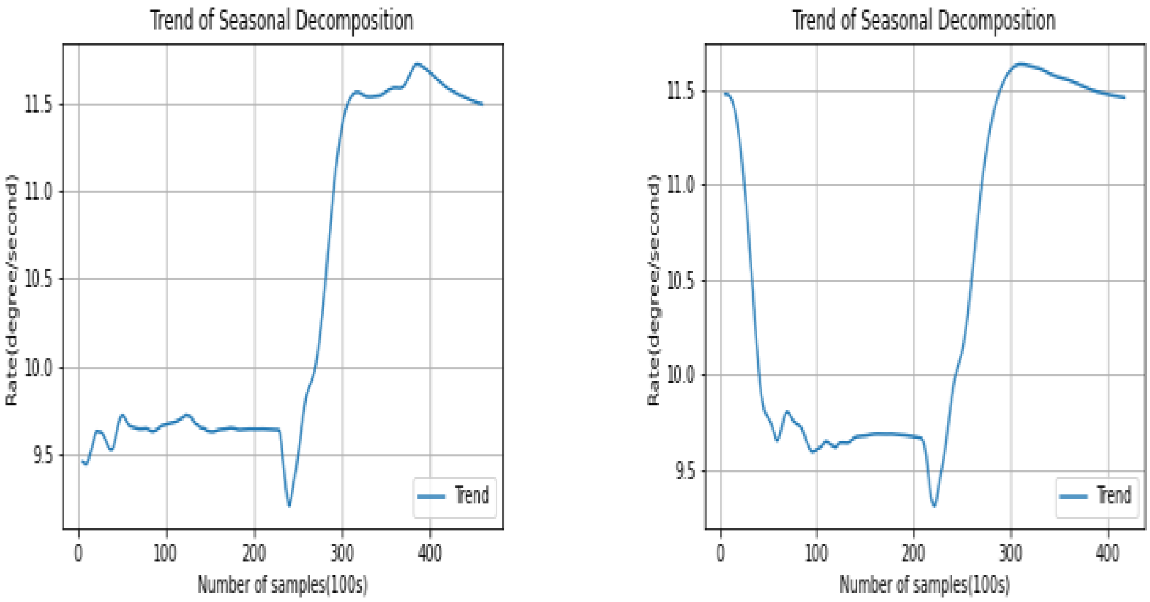

(a) Denoised Rate of first Thermal cycle

(b) Denoised Rate of second Thermal cycle

Figure 5.22: Denoised Rate of first and second thermal cycle.

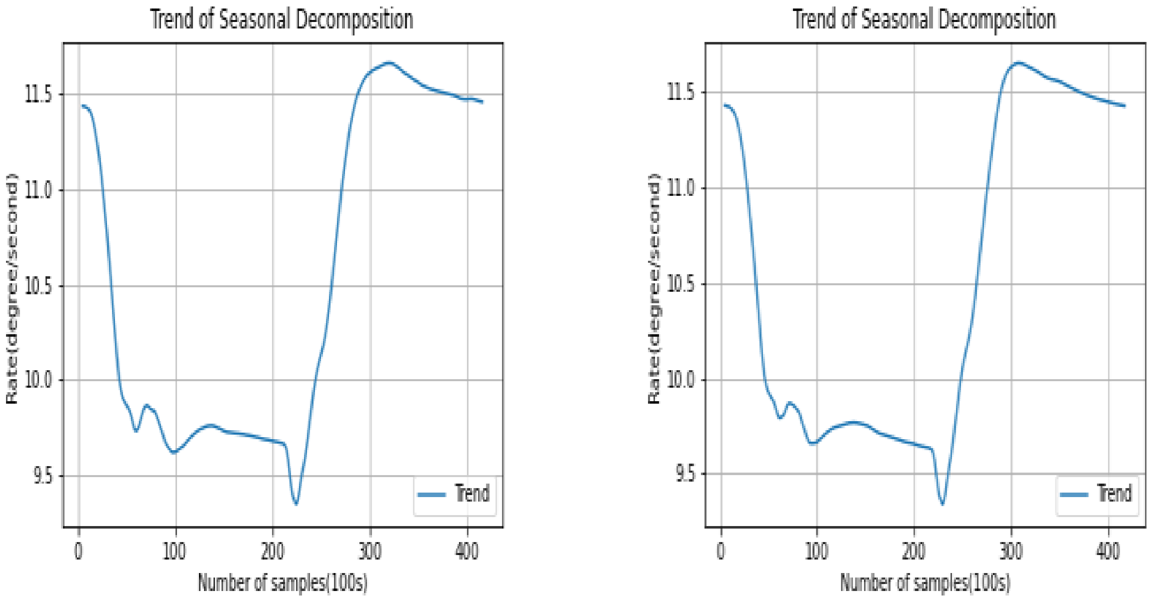

(a) Denoised Rate of third Thermal cycle

(b) Denoised Rate of Fourth Thermal cycle

Figure 5.23: Denoised Rate of third and fourth thermal cycle.

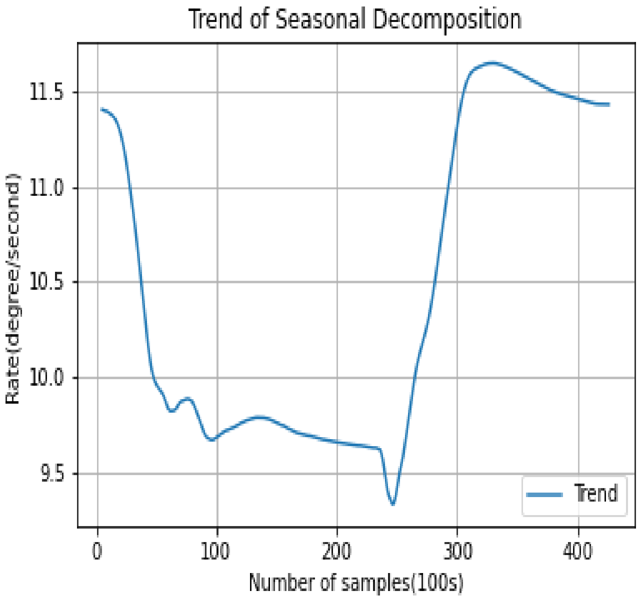

Figure 5.24: Denoised Rate of fifth thermal cycle.

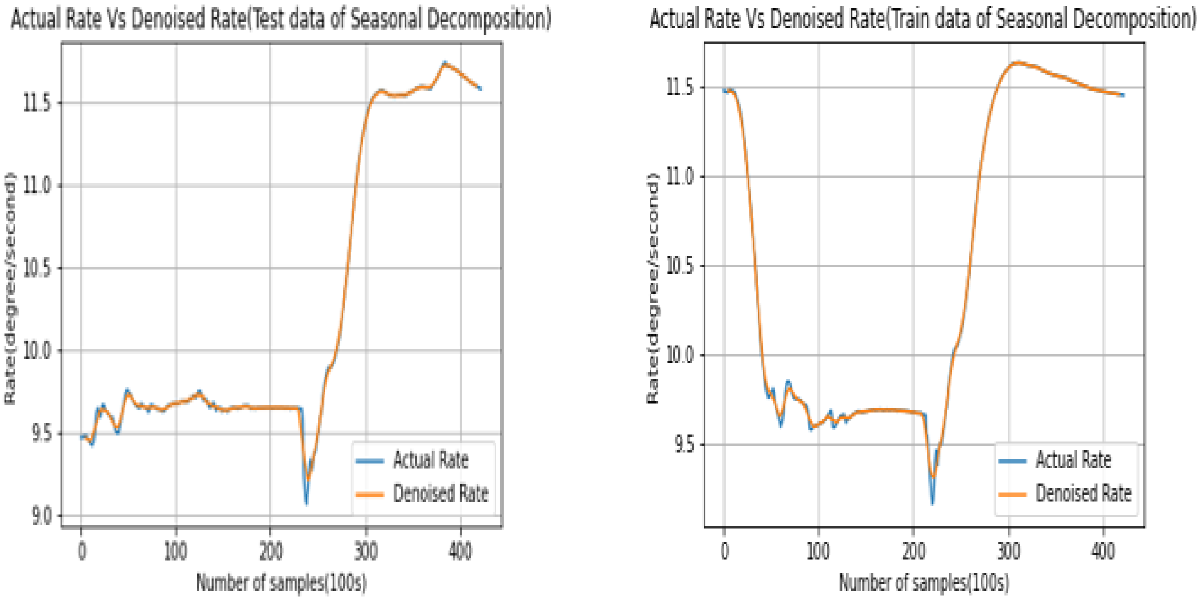

(a) Rate of first thermal cycle

(b) Rate of second Thermal cycle

Figure 5.25: Actual Rate Vs De-noised Rate of second and first thermal cycle of Seasonal Decomposition

.

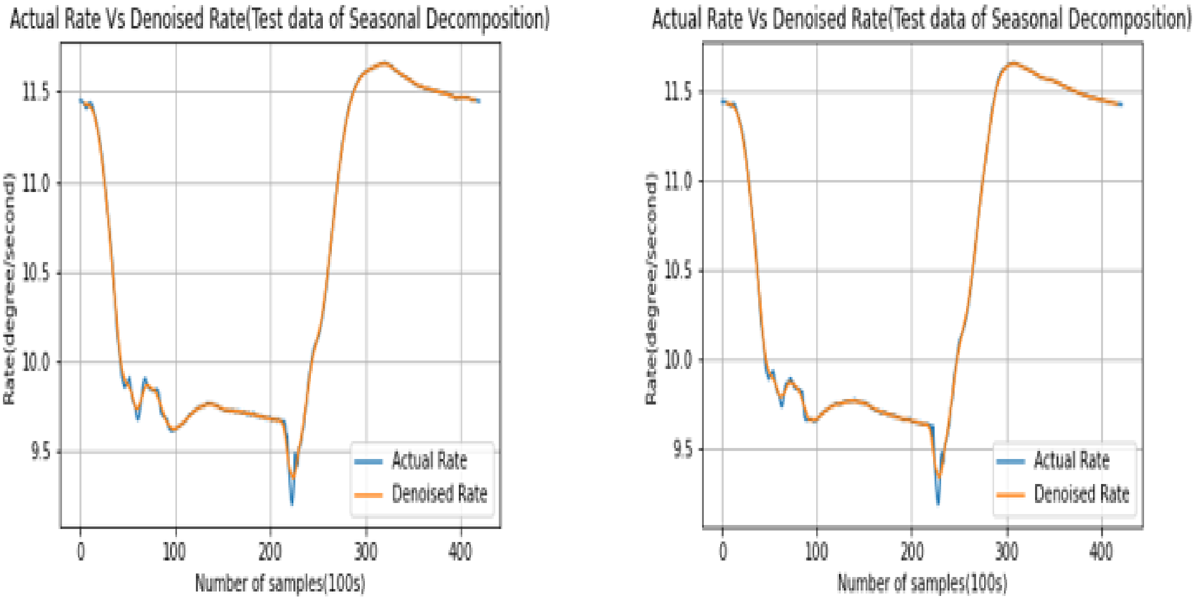

(a) Rate of third Thermal cycle

(b) Rate of Fourth Thermal cycle

Figure 5.26: Actual Rate Vs De-noised Rate of third and fourth thermal cycle.

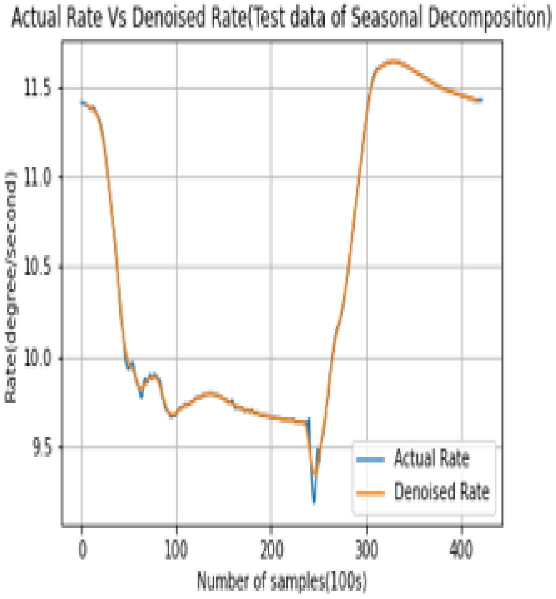

Figure 5.27: Actual Rate Vs De-noised Rate of fifth thermal cycle.

5.7 Seasonal Decomposition-LSTM

Based on the graph, it can be inferred that the seasonal component has a very low magnitude. Therefore, the trend component can be used for bias compensation using neural networks such as LSTM. The set of data used to train the model involves the amplitude and frequency of TFG during the initial thermal cycle, which is used as input for the LSTM neural network to fine-tune the model's hyperparameters.The remaining four thermal cycles, which include the denoised seasonal decomposition rate of TFG, are used as individual test data sets. This approach allows for four test data sets for comparison, which can be used to validate the effectiveness of the forecasting models. Figure 5.28 depicts the procedural framework of Seasonal-LSTM train data, while Figure 5.29 shows the procedural framework of Seasonal-LSTM test data.

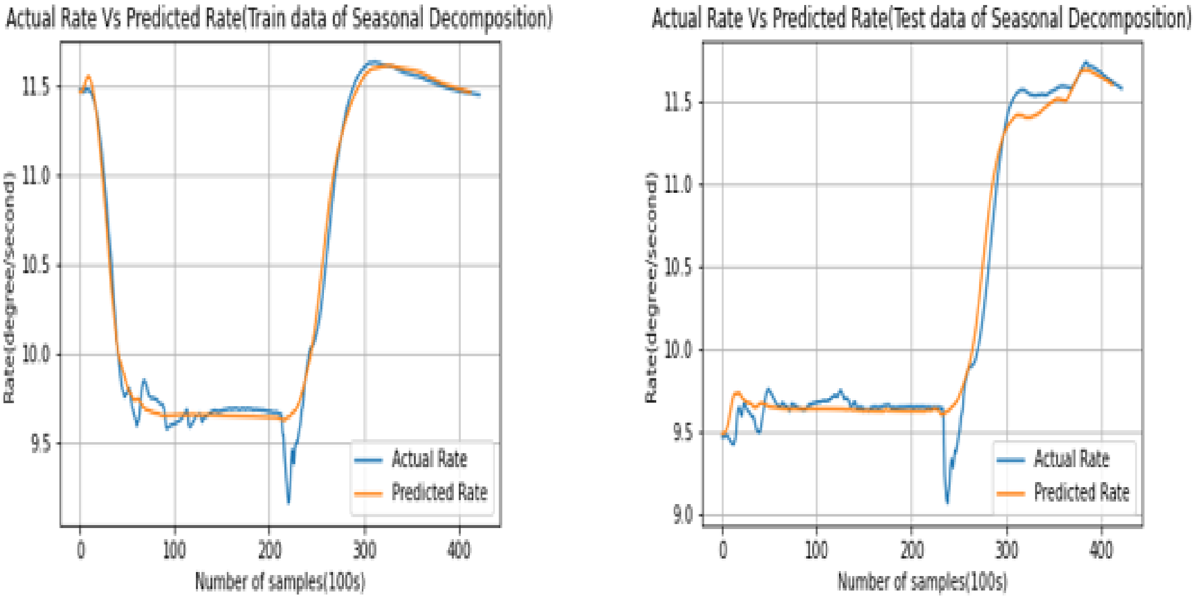

(a) Rate (Train data) of second thermal cycle

(b) Rate (Test data)of first Thermal cycle

Figure 5.28: Actual Rate Vs Predicted Rate of first and second thermal cycle of Seasonal Decomposition–LSTM.

Figure 5.30(a) shows Actual Rate Vs Predicted Rate (Train data) of the first thermal cycle of Seasonal Decomposi- tion–LSTM.From figure 5.30(b) to figure 5.32(b) shows the Actual Rate Vs Predicted Rate(test data) of second,third,fourth,fifth thermal cycles of Seasonal Decomposi- tion–LSTM respectively.

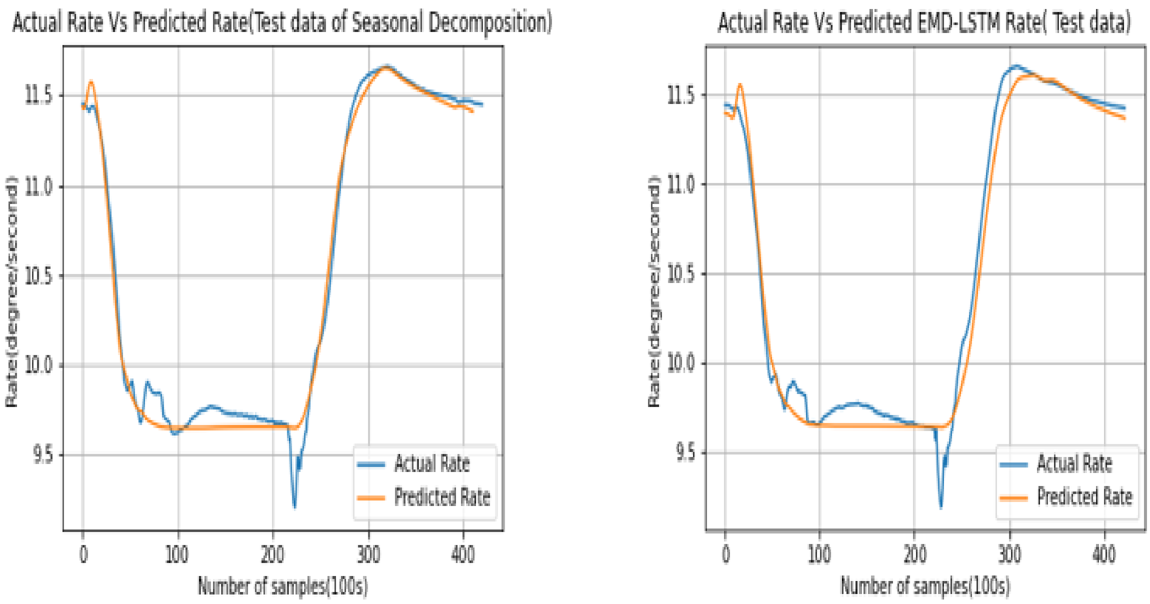

(a) Rate (Test data)of third Thermal cycle

(b) Rate (Test data) of Fourth Thermal cycle

Figure 5.29: Actual Rate Vs Predicted Rate of third and fourth thermal cycle of Seasonal Decomposition–LSTM.

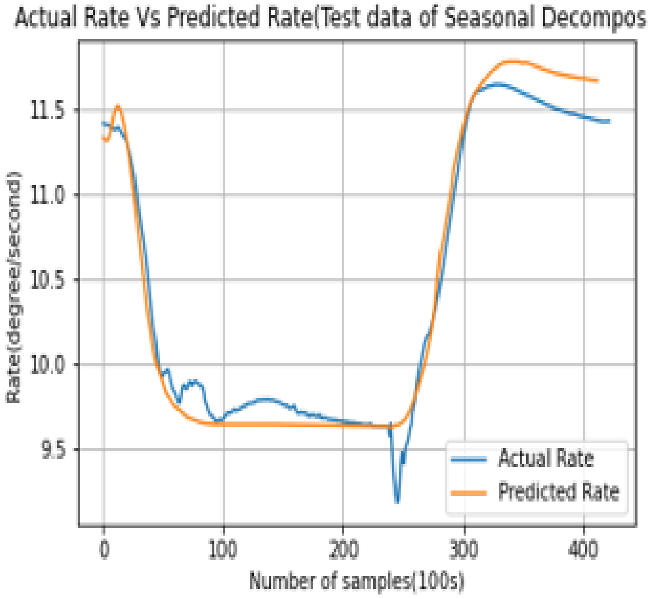

Figure 5.30: Actual Rate Vs Predicted Rate (Test data) of fifth thermal cycle of Seasonal Decomposition–LSTM.

5.8 Empirical Mode Decomposition

EMD is used to analyze non-linear and non-stationery signals by separating them into components at different resolutions. It decomposes the data into small number of different Intrinsic Mode functions(IMFs) and a residue.

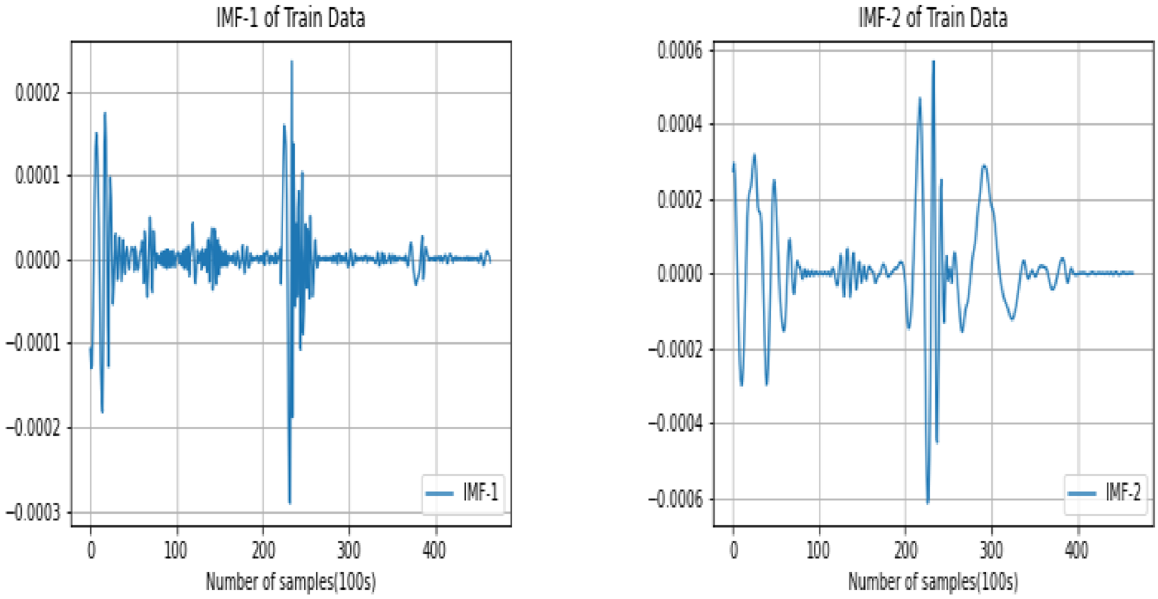

(a) IMF-1 of first thermal cycle

(b) IMF-2 of first thermal cycle

Figure 5.31: Intrinsic Mode Functions(IMFs) of first thermal cycle

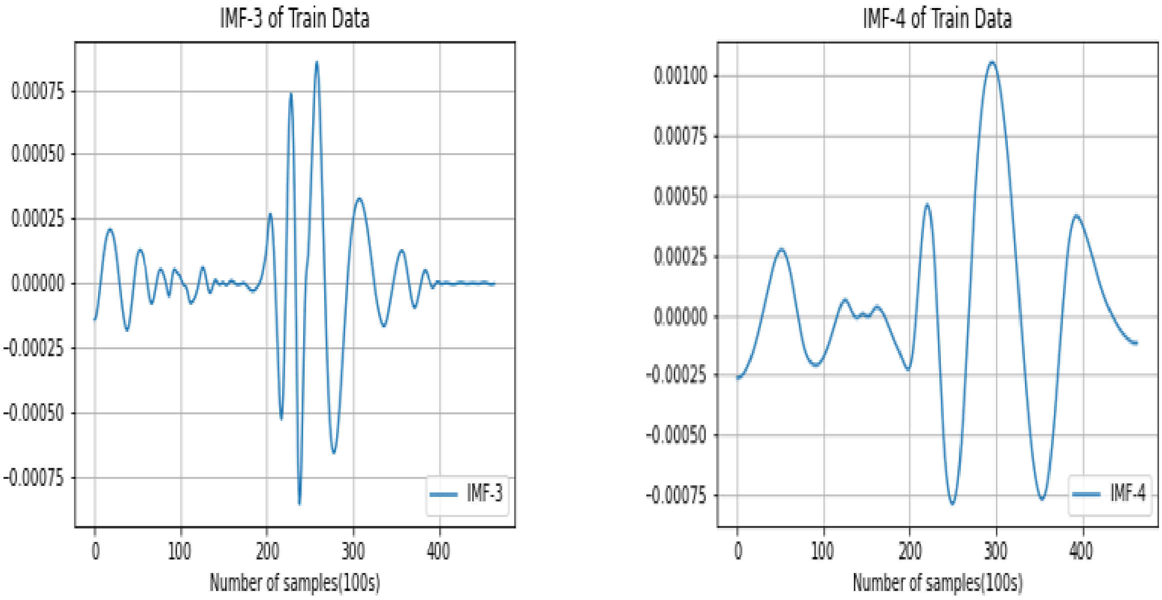

(a) IMF-3 of first thermal cycle

(b) IMF-4 of first thermal cycle

Figure 5.32: Intrinsic Mode Functions(IMFs) of first thermal cycle

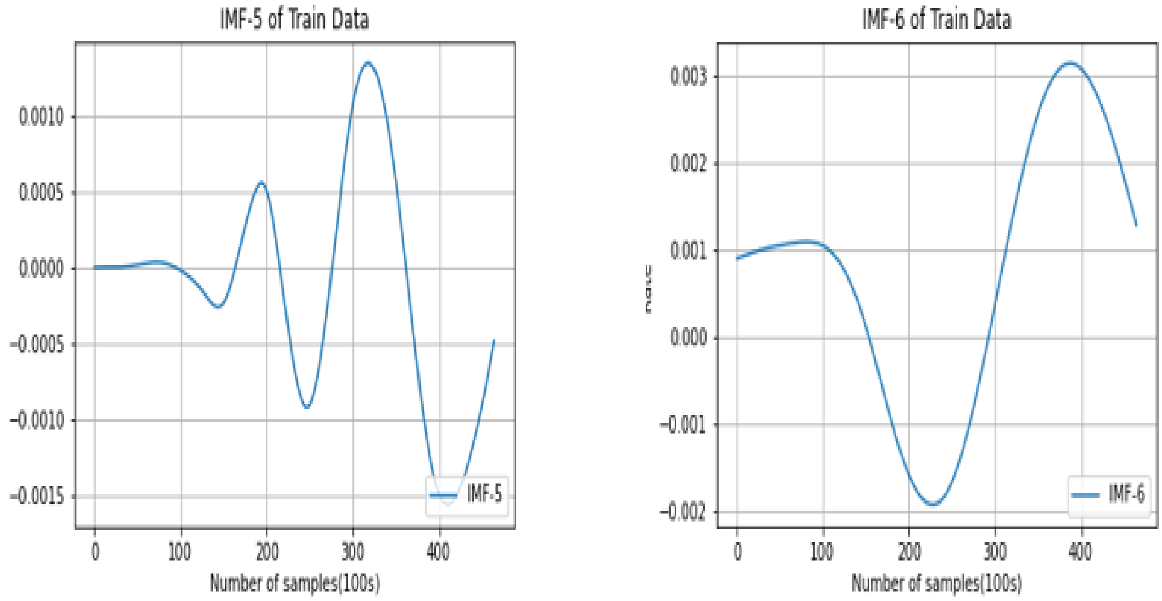

(a) IMF-5 of first thermal cycle

(b) IMF-6 of first thermal cycle

Figure 5.33: Intrinsic Mode Functions(IMFs) of first thermal cycle

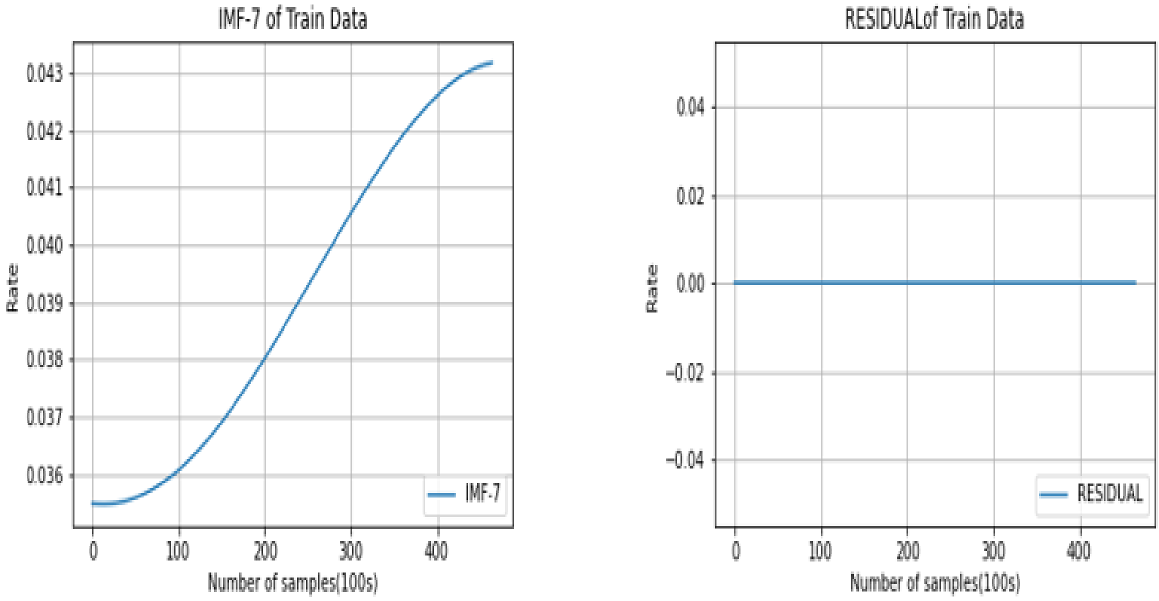

(a) IMF-7 of first thermal cycle

(b) Residual of first thermal cycle

Figure 5.34: Intrinsic Mode Functions(IMFs) and residual of first thermal cycle

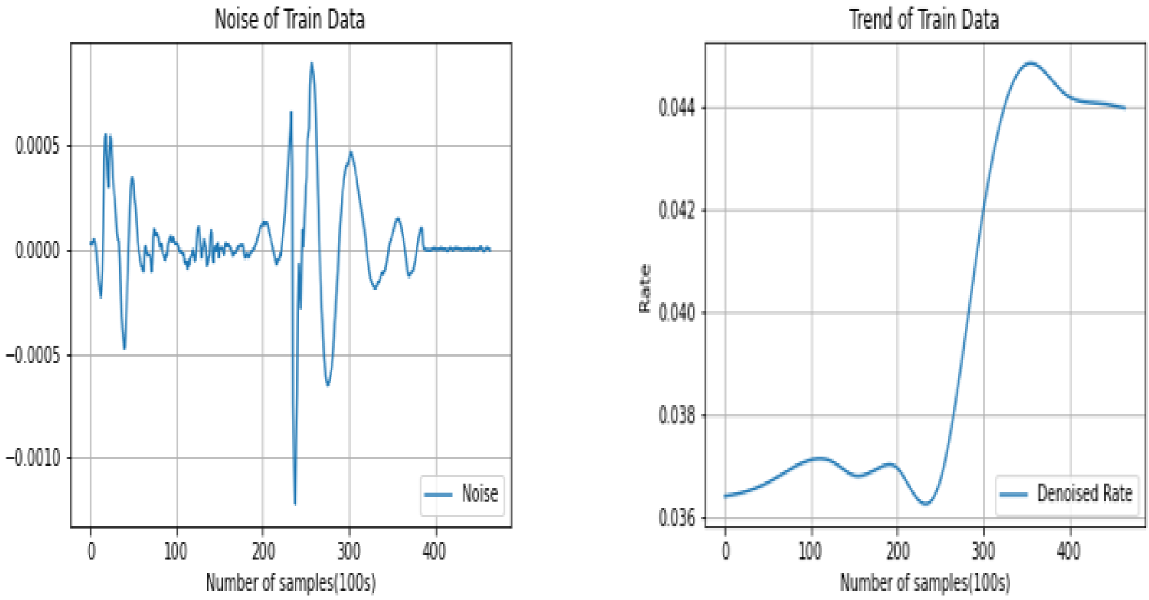

(a) Noise of first thermal cycle

(b) Denoised Rate of first thermal cycle

Figure 5.35: Noise Vs Denoised rate of first thermal cycle

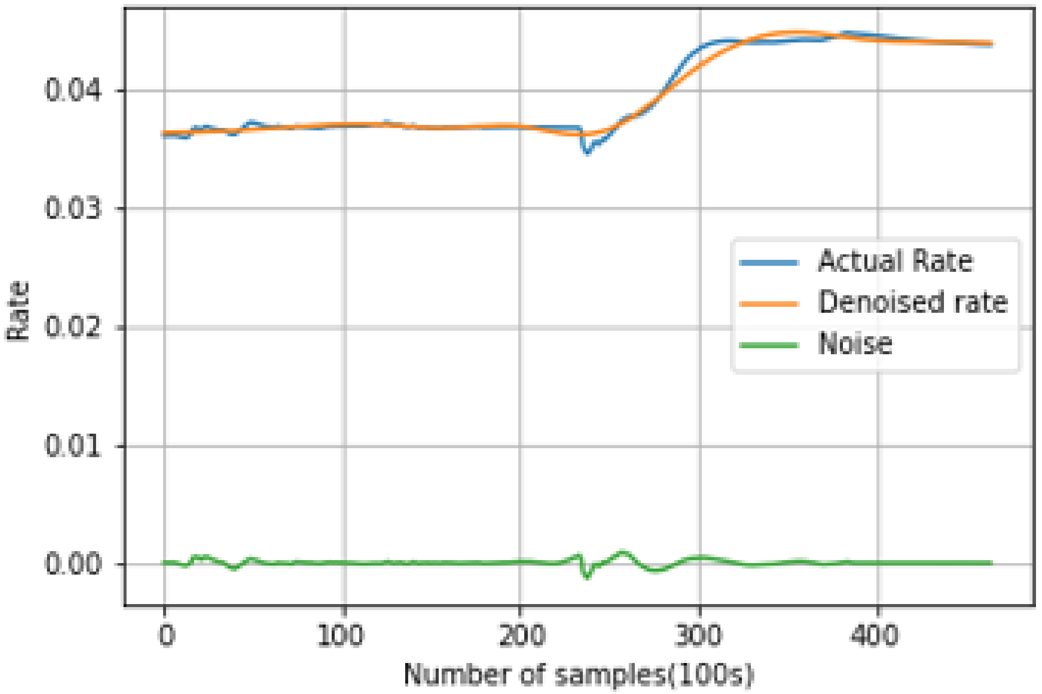

Figure 5.36: Denoising of first thermal cycle

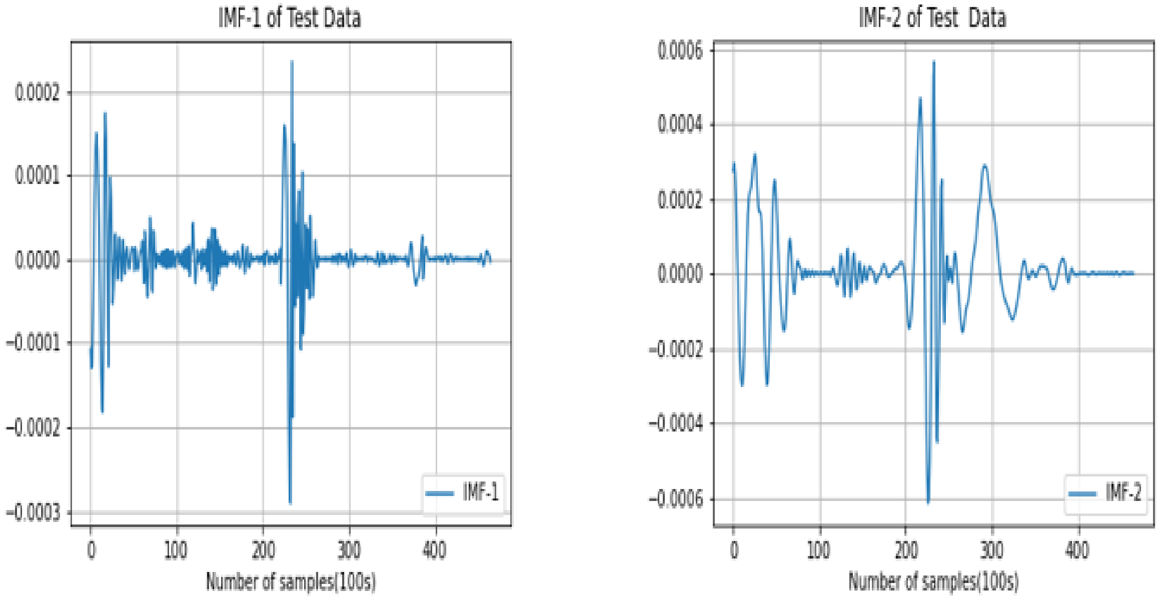

(a) IMF-1 of Second thermal cycle

(b) IMF-2 of Second thermal cycle

Figure 5.37: Intrinsic Mode Functions(IMFs) of Second thermal cycle

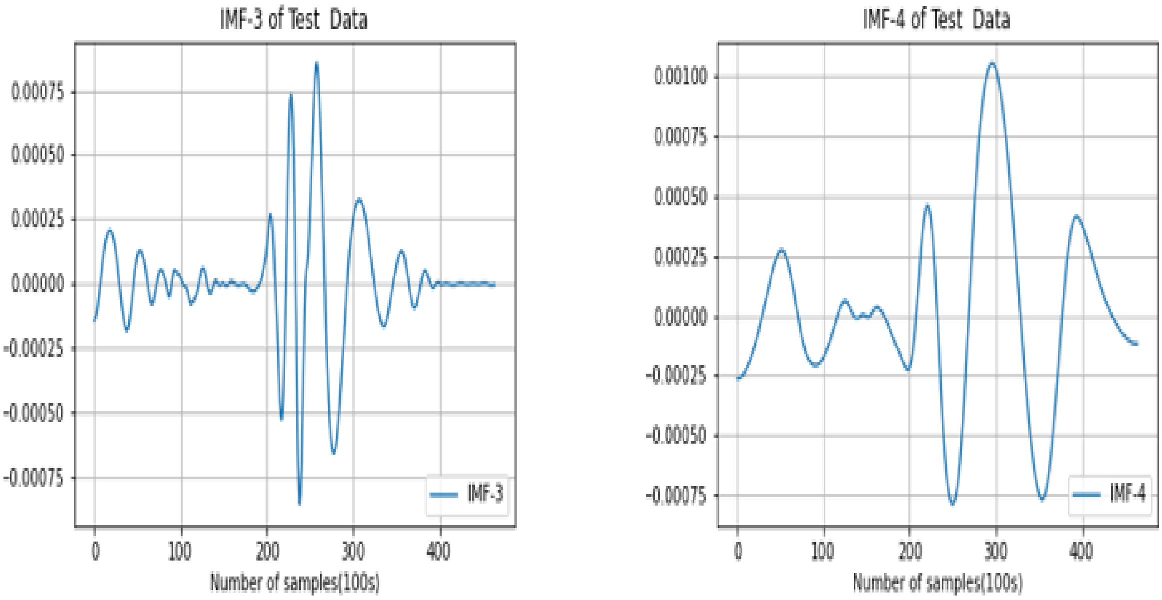

(a) IMF-3 of Second thermal cycle

(b) IMF-4 of Second thermal cycle

Figure 5.38: Intrinsic Mode Functions(IMFs) of Second thermal cycle

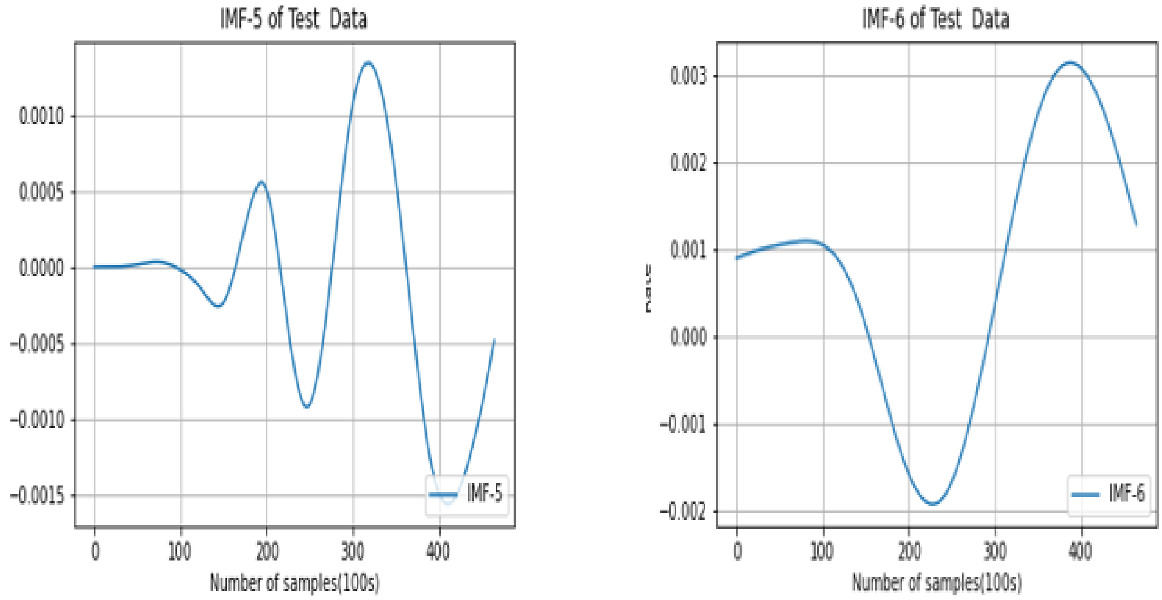

(a) IMF-5 of Second thermal cycle

(b) IMF-6 of Second thermal cycle

Figure 5.39: Intrinsic Mode Functions(IMFs) of Second thermal cycle

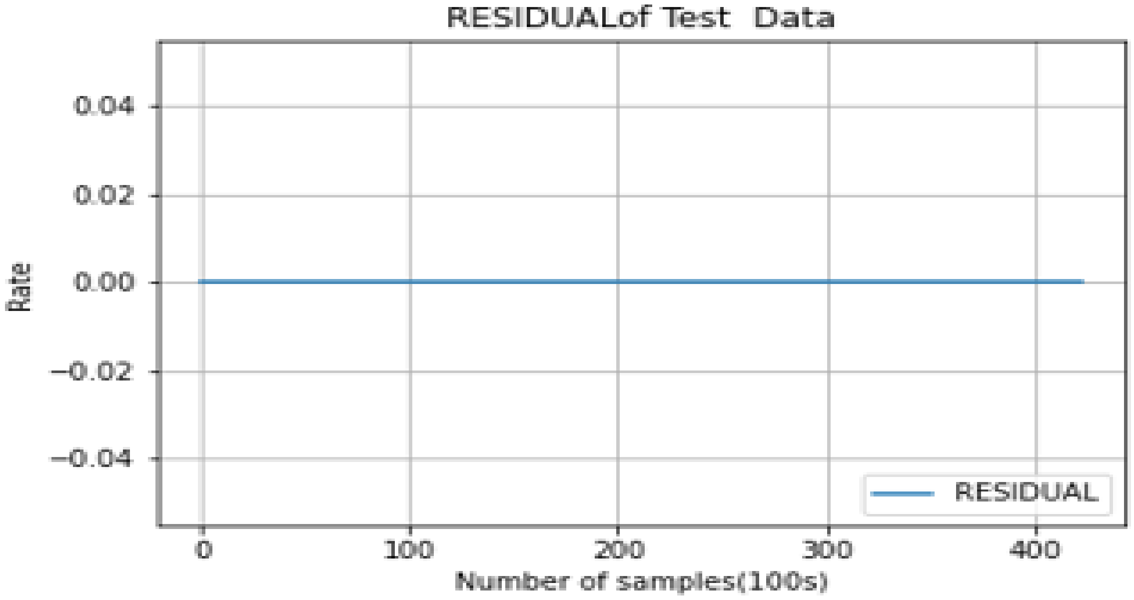

Figure 5.40: Residual of Second thermal cycle

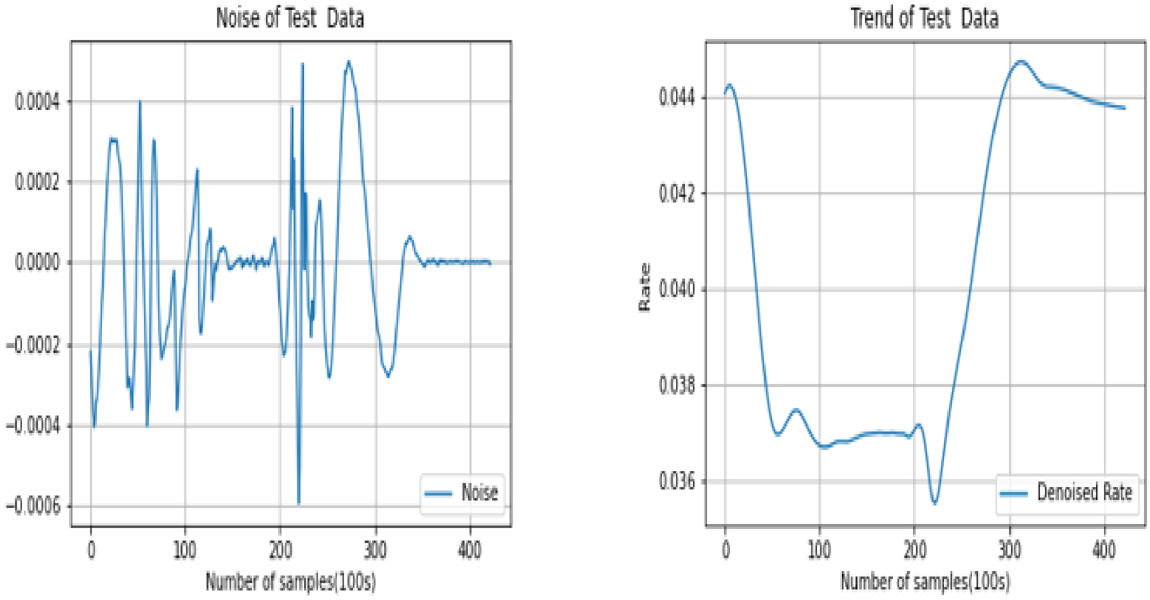

(a) Noise of Second thermal cycle

(b) Denoised Rate of first thermal cycle

Figure 5.41: Noise Vs Denoised rate of Second thermal cycle

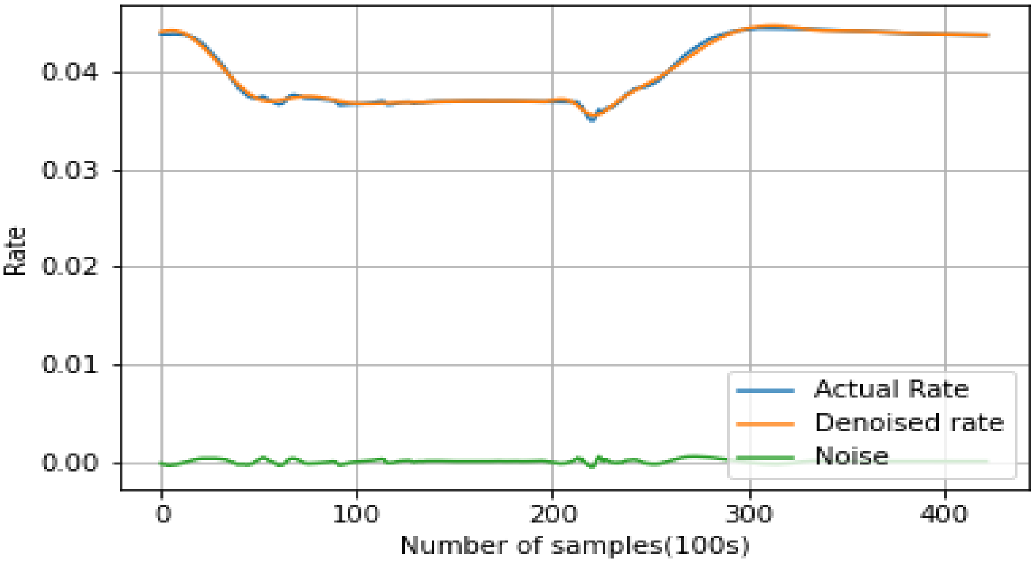

Figure 5.42: Denoising of Second thermal cycle

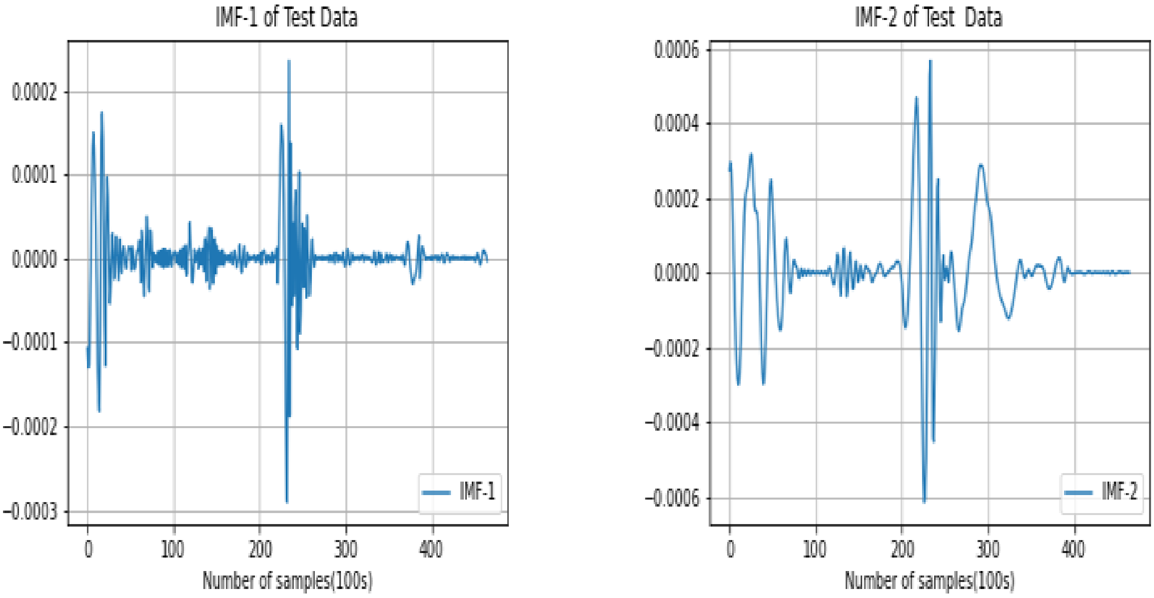

(a) IMF-1 of Third thermal cycle

(b) IMF-2 of Third thermal cycle

Figure 5.43: Intrinsic Mode Functions(IMFs) of Third thermal cycle

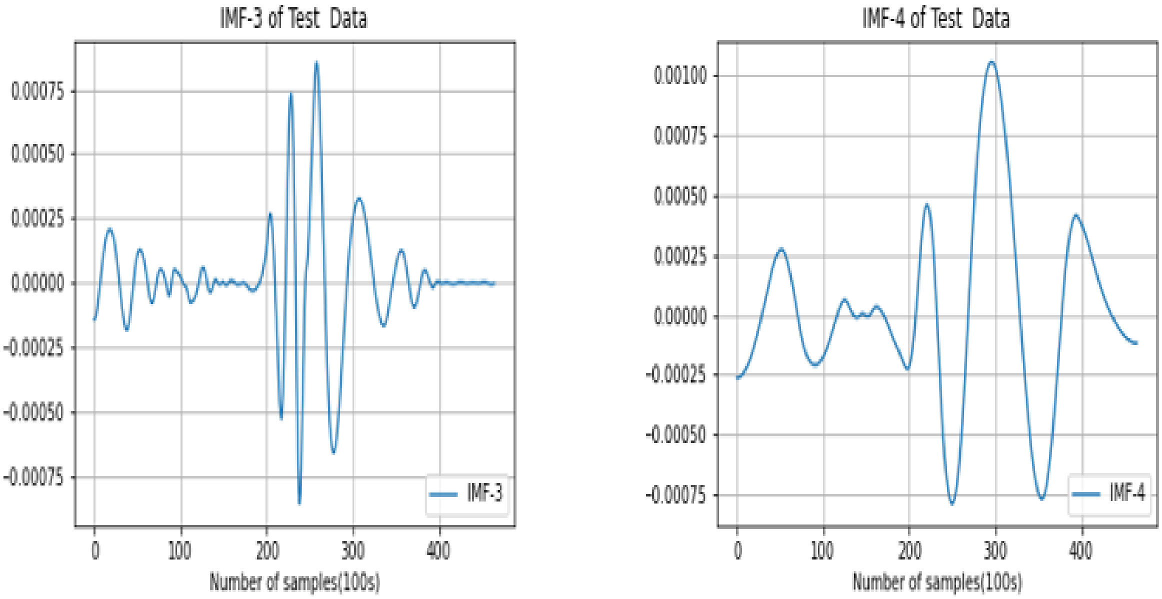

(a) IMF-3 of Third thermal cycle

(b) IMF-4 of Third thermal cycle

Figure 5.44: Intrinsic Mode Functions(IMFs) of Third thermal cycle

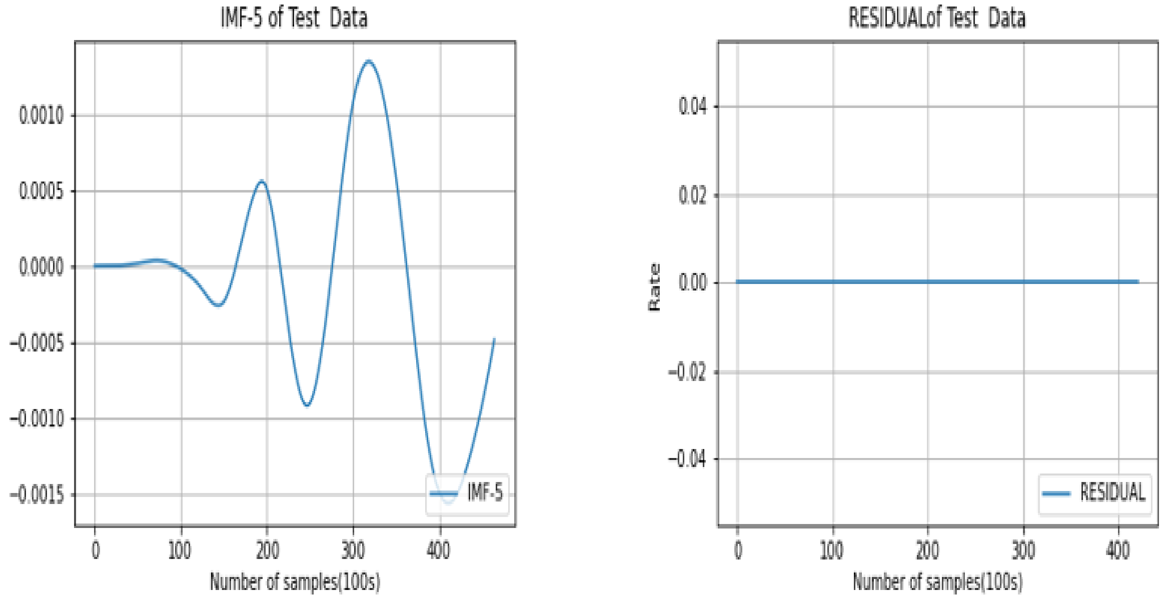

(a) IMF-5 of Third thermal cycle

(b) Residual of Third thermal cycle

Figure 5.45: Intrinsic Mode Functions(IMFs) Residual of Third thermal cycle

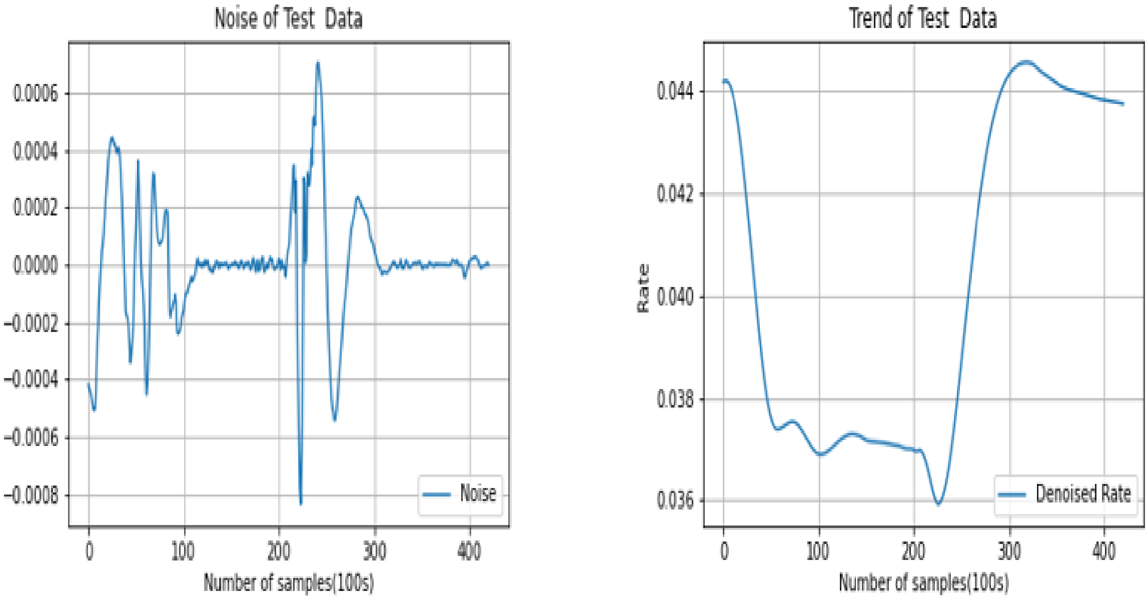

(a) Noise of Third thermal cycle

(b) Denoised Rate of Third thermal cycle

Figure 5.46: Noise Vs Denoised rate of Third thermal cycle

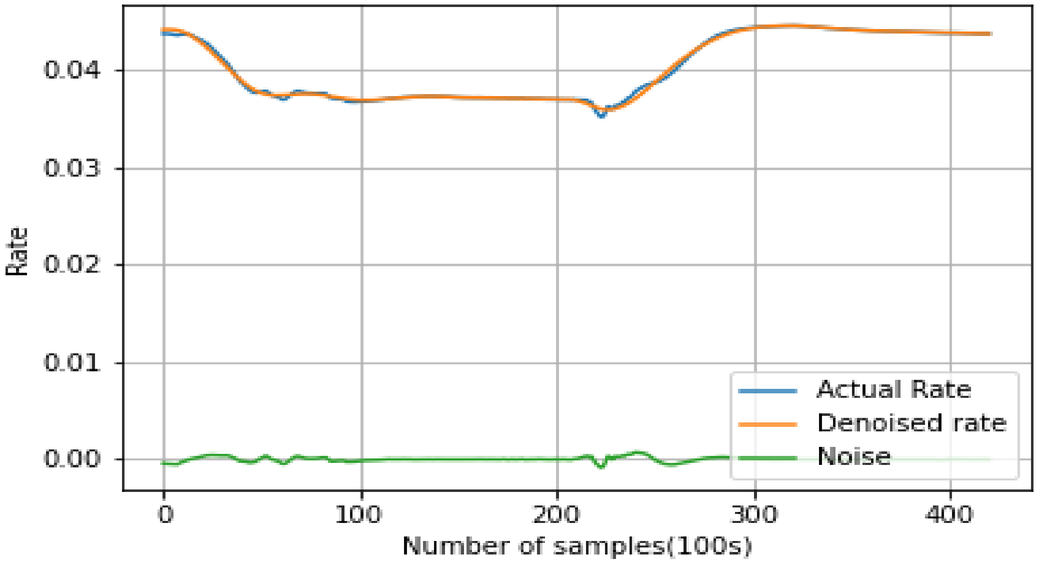

Figure 5.47: Denoising of Third thermal cycle

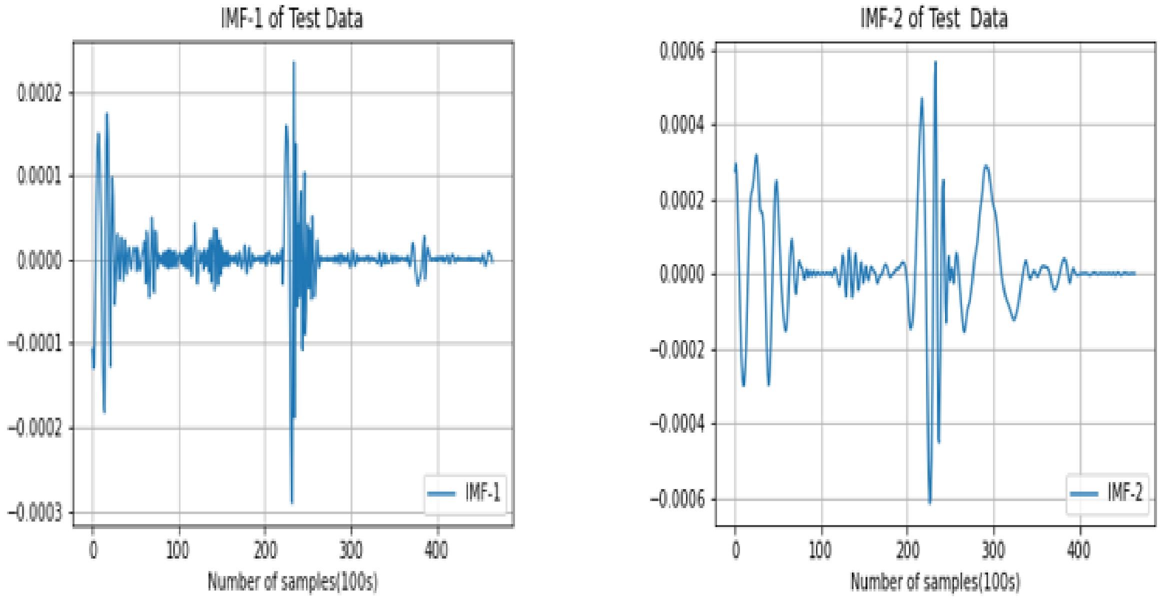

(a) IMF-1 of fourth thermal cycle

(b) IMF-2 of fourth thermal cycle

Figure 5.48: Intrinsic Mode Functions(IMFs) of fourth thermal cycle

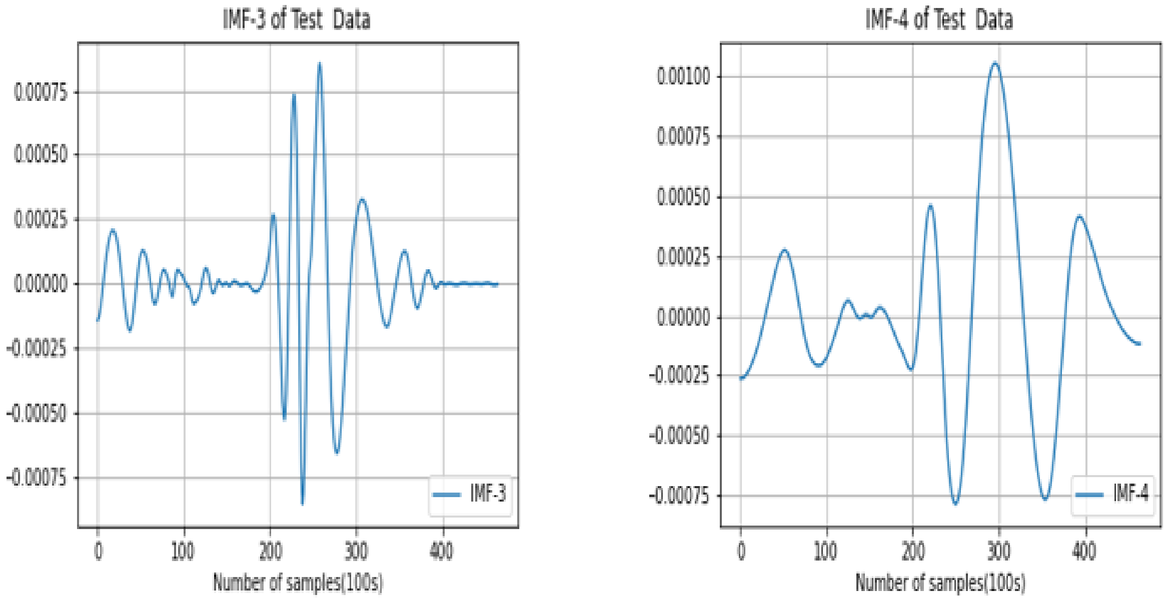

(a) IMF-3 of fourth thermal cycle

(b) IMF-4 of fourth thermal cycle

Figure 5.49: Intrinsic Mode Functions(IMFs) of fourth thermal cycle

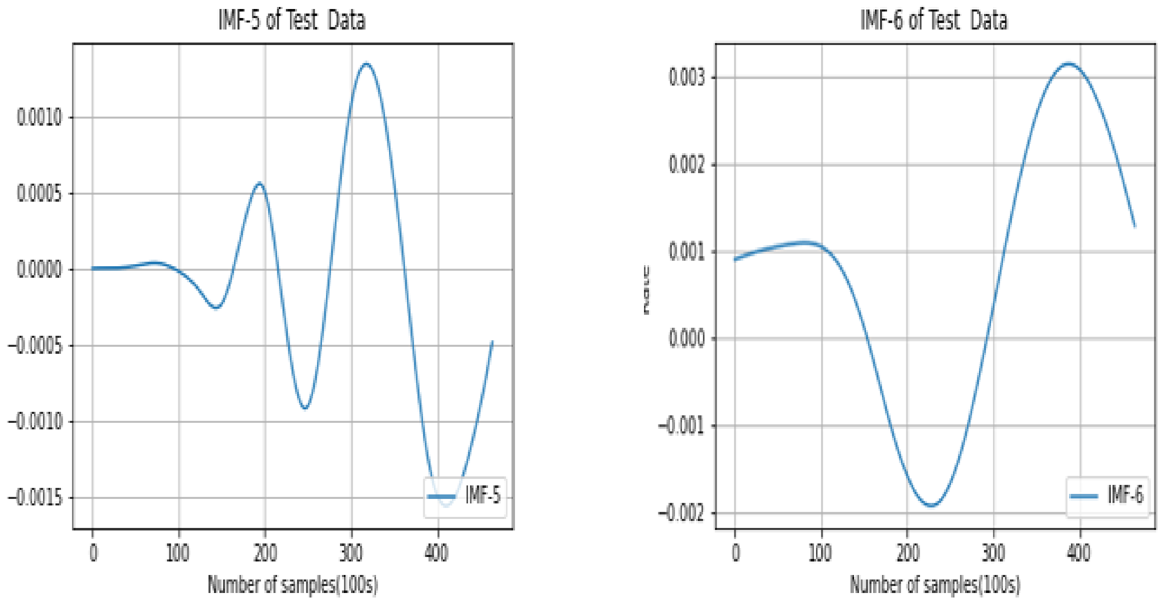

(a) IMF-5 of fourth thermal cycle

(b) IMF-6 of fourth thermal cycle

Figure 5.50: Intrinsic Mode Functions(IMFs) of fourth thermal cycle

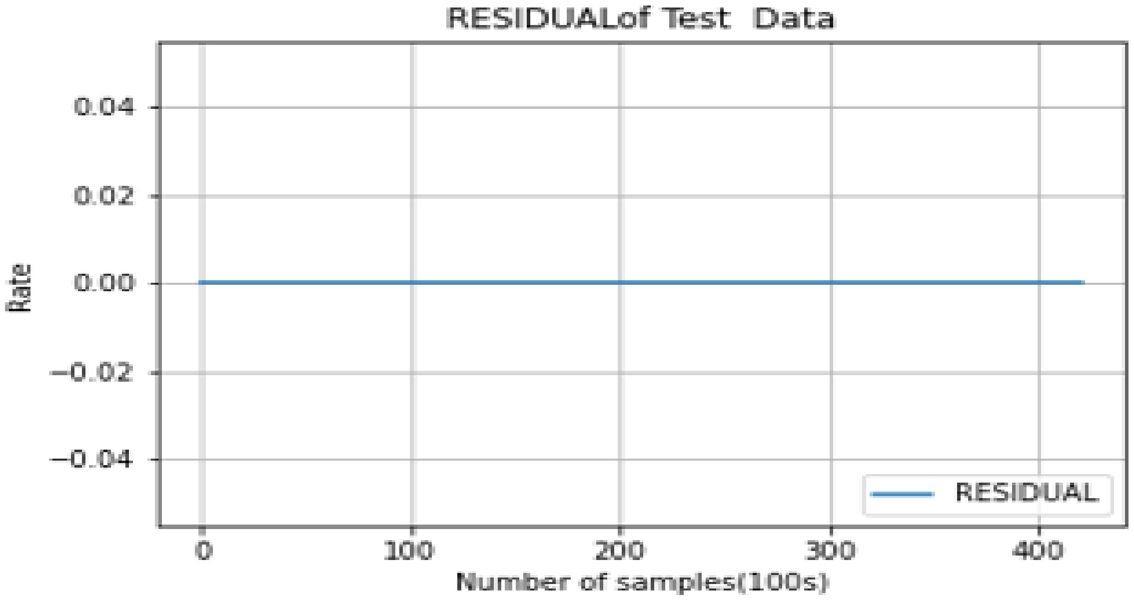

Figure 5.51: Residual of fourth thermal cycle

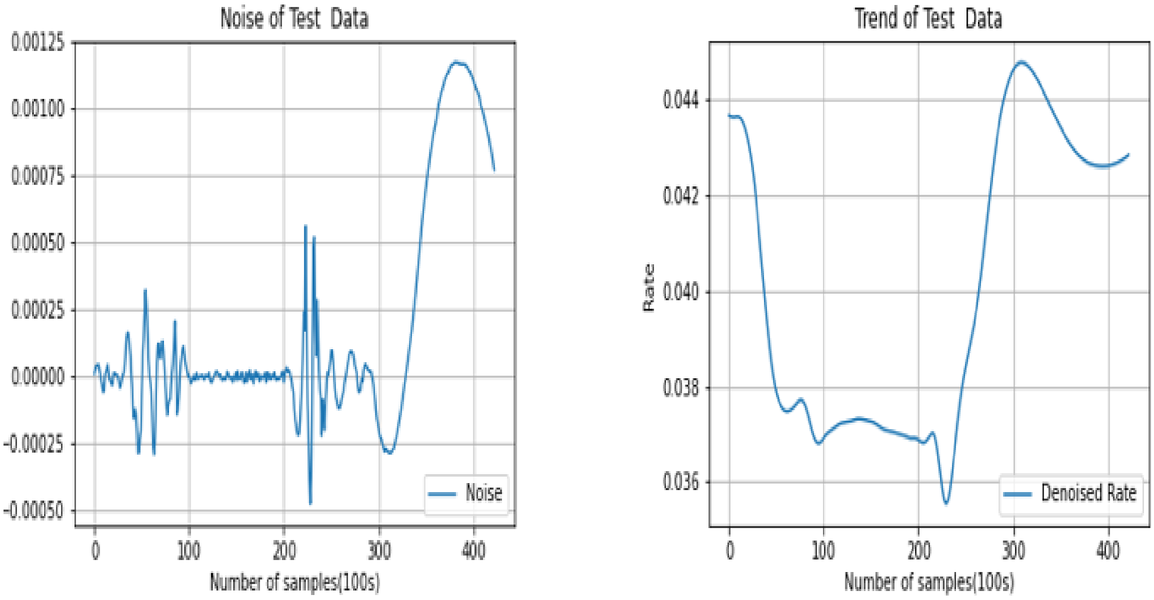

(a) Noise of fourth thermal cycle

(b) Denoised Rate of fourth thermal cycle

Figure 5.52: Noise Vs Denoised rate of fourth thermal cycle

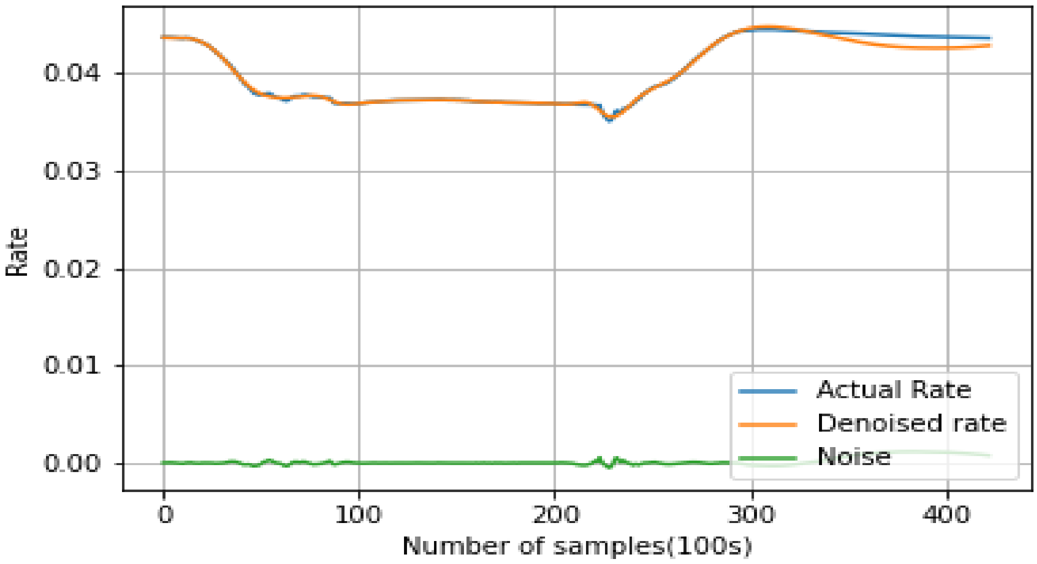

Figure 5.53: Denoising of fourth thermal cycle

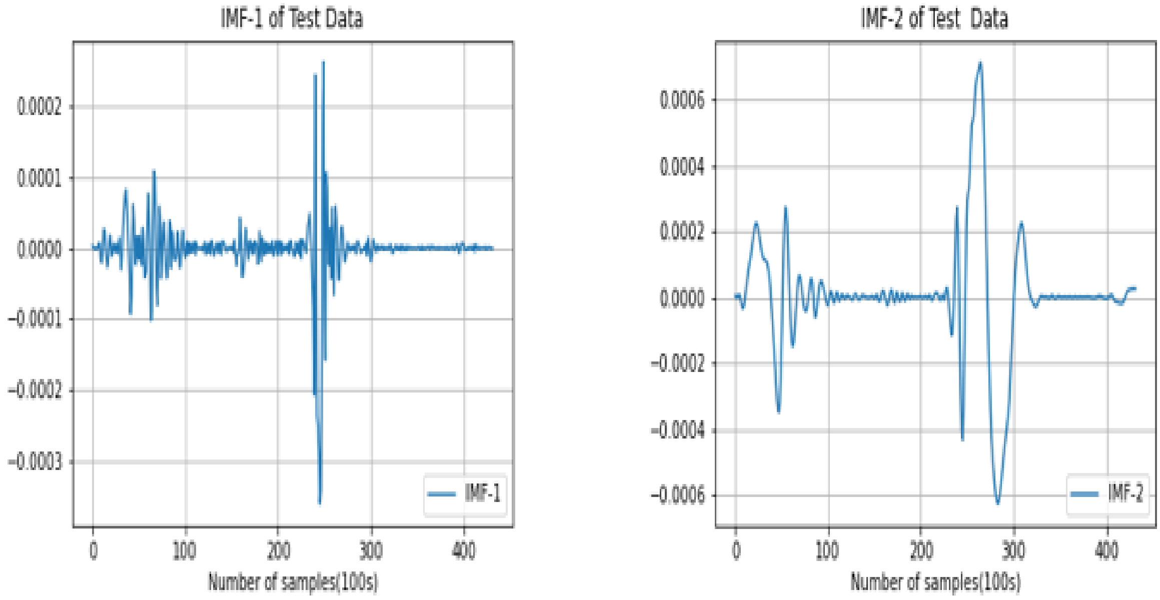

(a) IMF-1 of fifth thermal cycle

(b) IMF-2 of fifth thermal cycle

Figure 5.54: Intrinsic Mode Functions(IMFs) of fifth thermal cycle

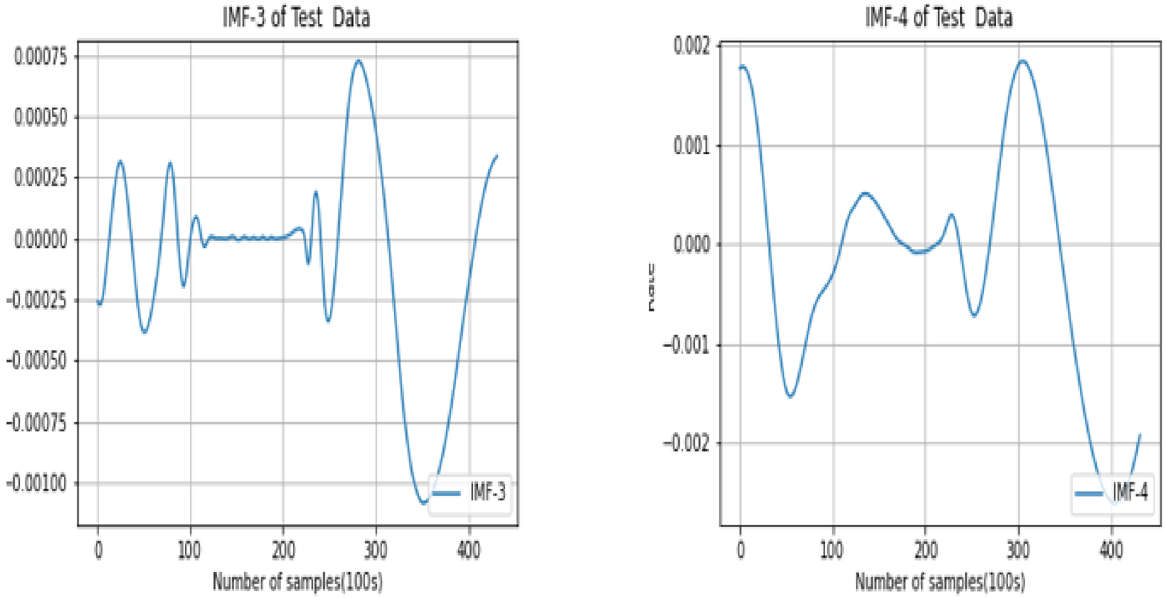

(a) IMF-3 of fifth thermal cycle

(b) IMF-4 of fifth thermal cycle

Figure 5.55: Intrinsic Mode Functions(IMFs) of fifth thermal cycle

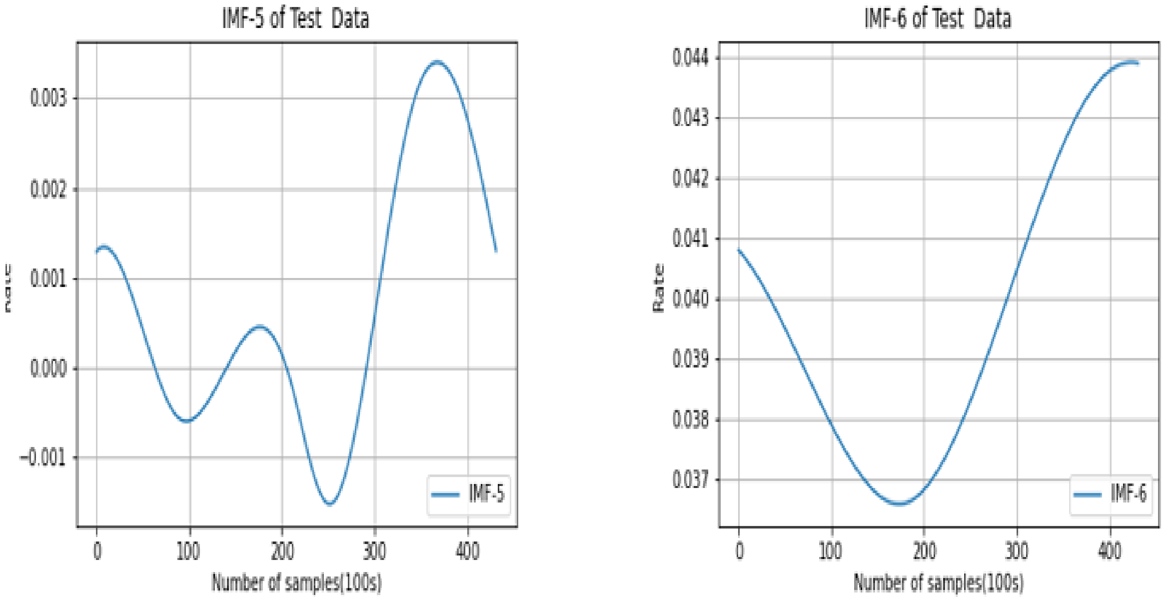

(a) IMF-5 of fifth thermal cycle

(b) IMF-6 of fifth thermal cycle

Figure 5.56: Intrinsic Mode Functions(IMFs) of fifth thermal cycle

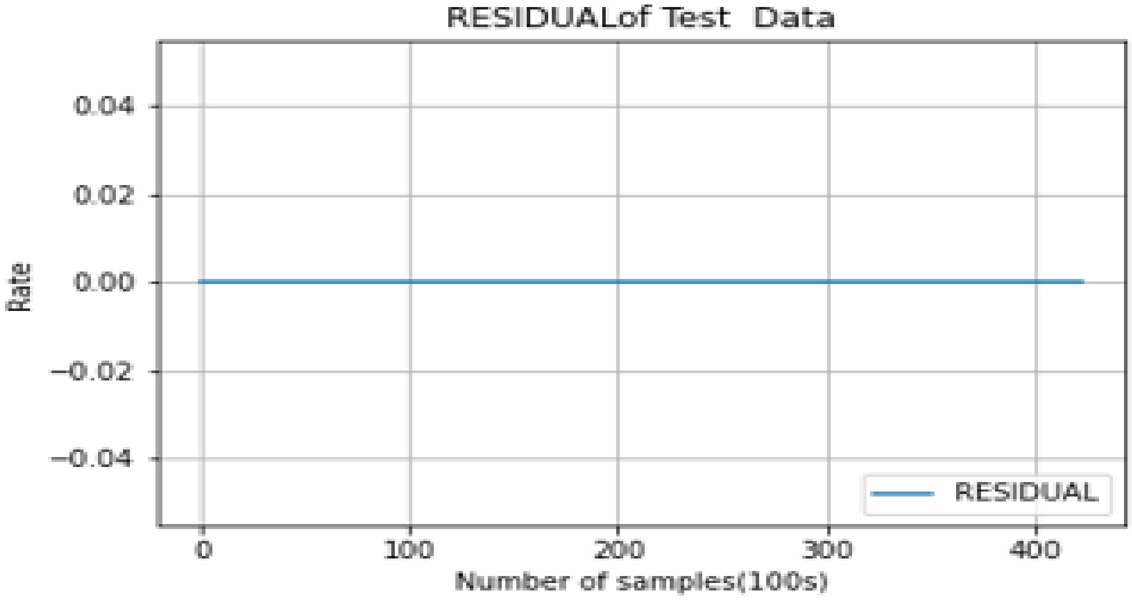

Figure 5.57: Residual of fifth thermal cycle

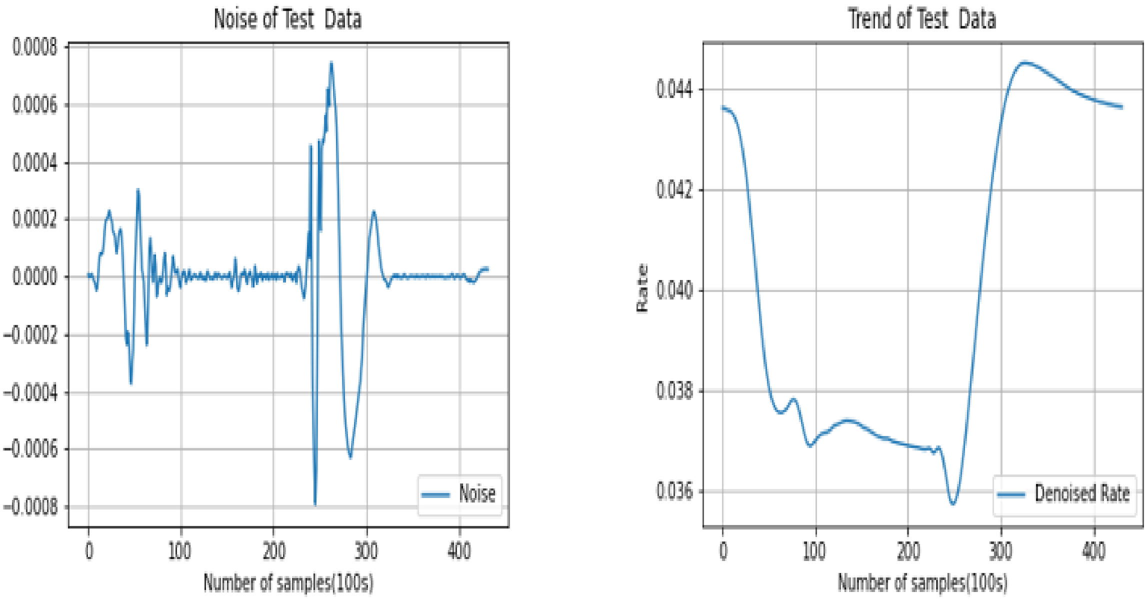

(a) Noise of fifth thermal cycle

(b) Denoised Rate of fifth thermal cycle

Figure 5.58: Noise Vs Denoised rate of fifth thermal cycle

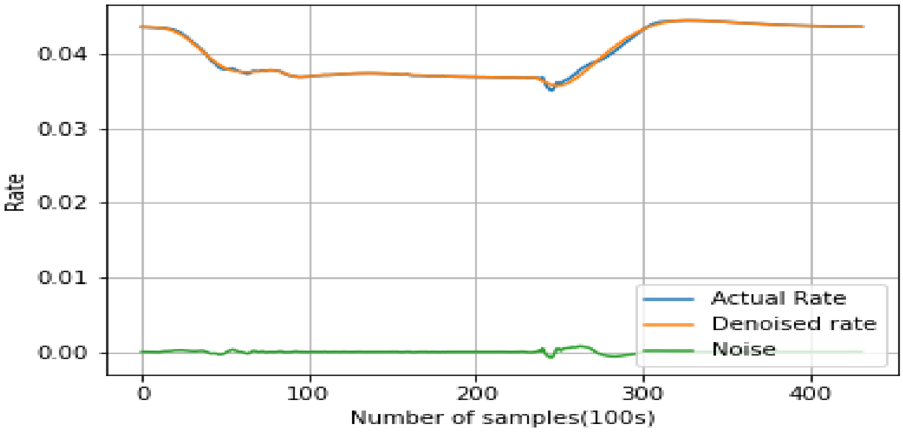

Figure 5.59: Denoising of fifth thermal cycle

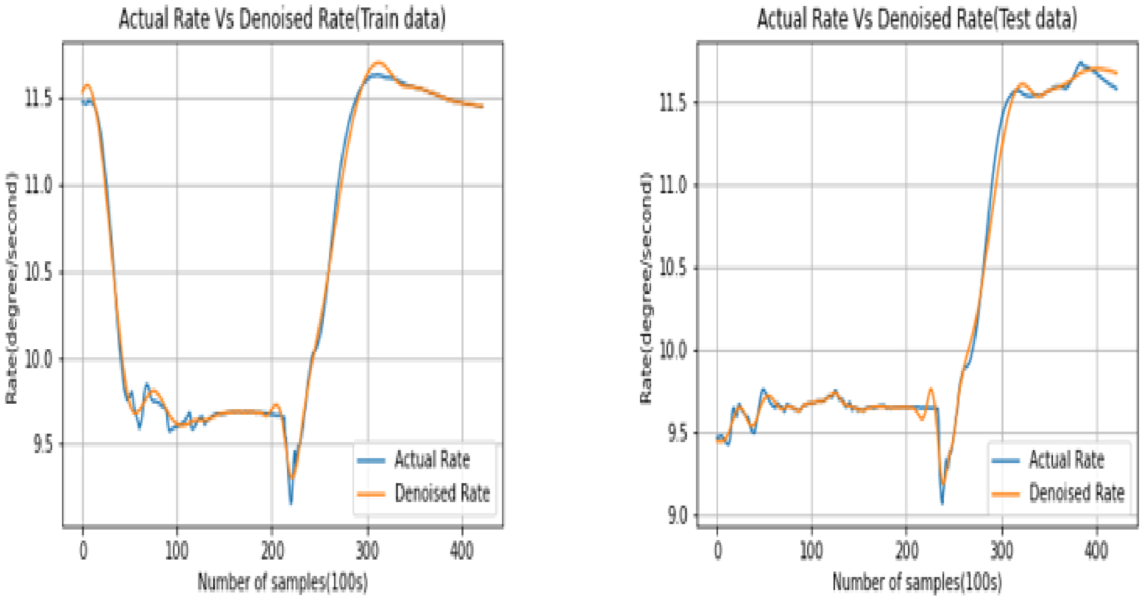

(a) Actual Rate Vs Denoised Rate of EMD

(b) Actual Rate Vs Denoised Rate of EMD

Figure 5.60: Actual Rate Vs EMD Denoised Rate of Second and First thermal cycle.

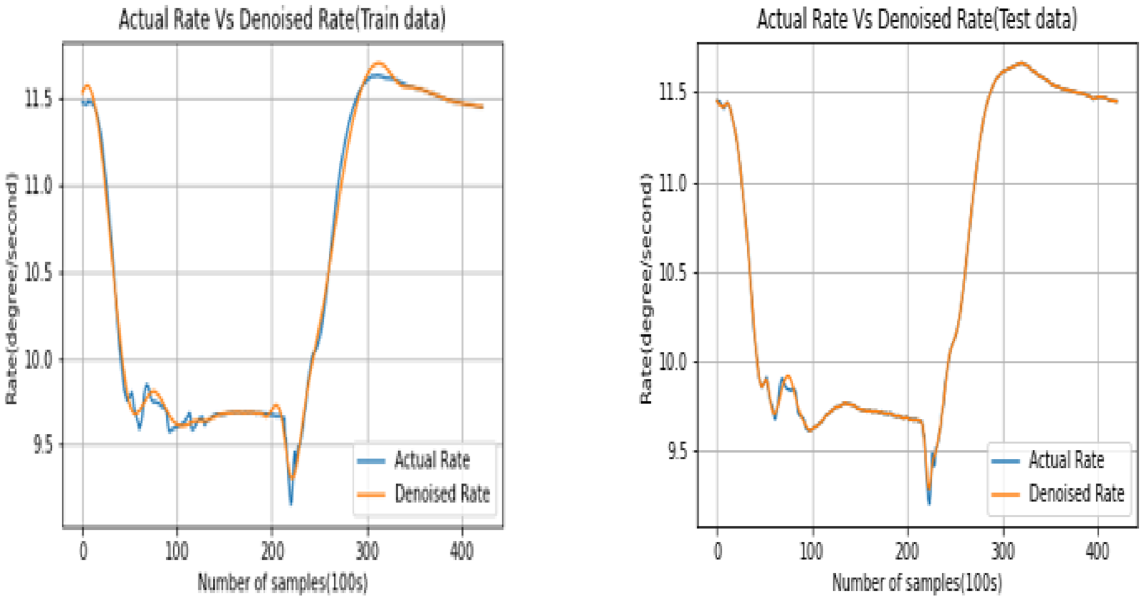

(a) Actual Rate Vs Denoised Rate of EMD

(b) Actual Rate Vs Denoised Rate of EMD

Figure 5.61: Actual Rate Vs EMD Denoised Rate of Second and third thermal cycle.

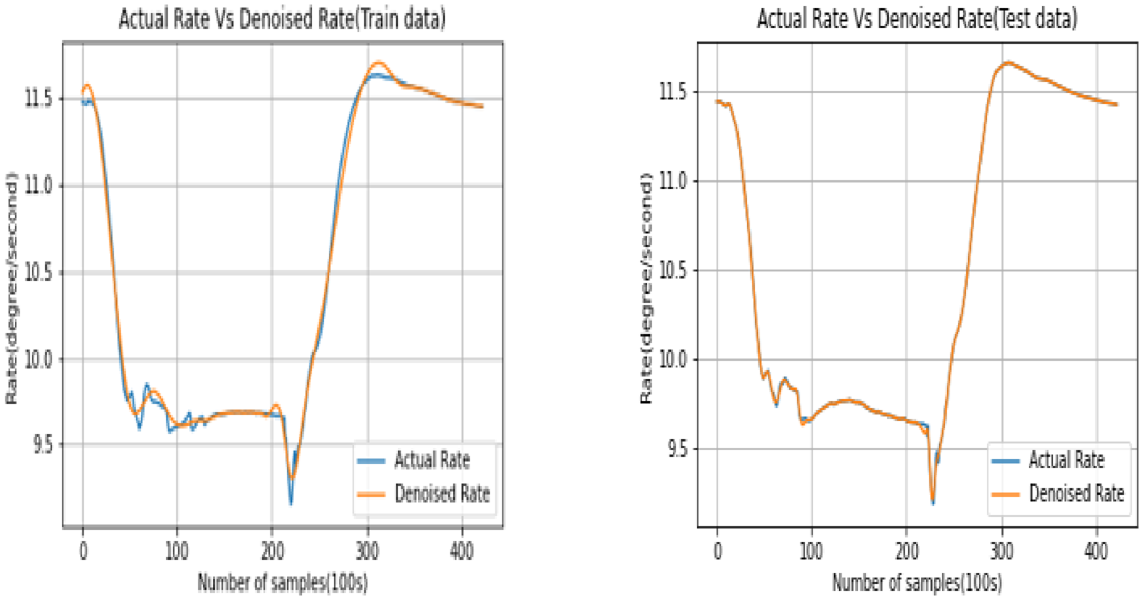

(a) Actual Rate Vs Denoised Rate of EMD

(b) Actual Rate Vs Denoised Rate of EMD

Figure 5.62: Actual Rate Vs EMD Denoised Rate of Second and fourth thermal cycle.

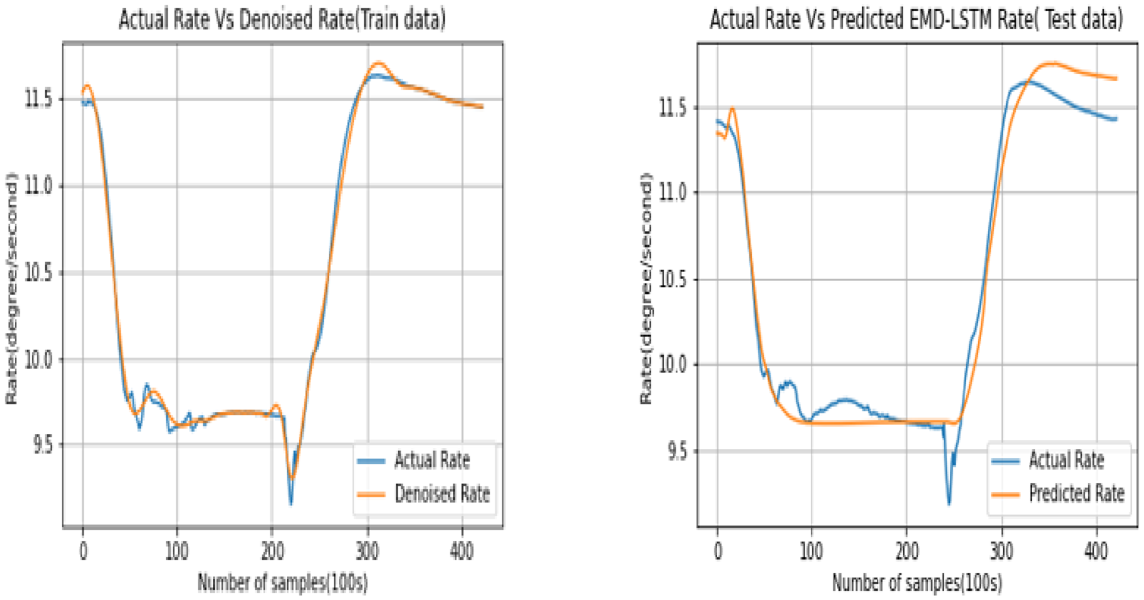

(a) Actual Rate Vs Denoised Rate of EMD

(b) Actual Rate Vs Denoised Rate of EMD

Figure 5.63: Actual Rate Vs EMD Denoised Rate of First and fifth thermal cycle.

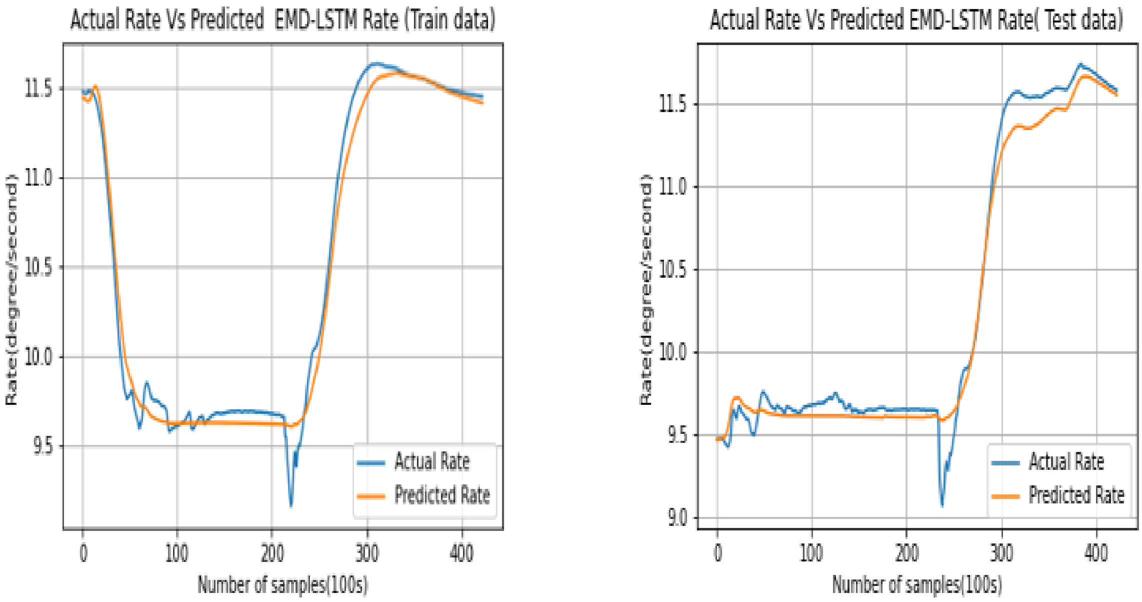

(a) Actual Rate Vs Predicted Rate of EMD-LSTM (b) Actual Rate Vs Predicted Rate of EMD-LSTM

Figure 5.64: Actual Rate Vs EMD-LSTM Predicted Rate of second and First thermal cycle.

5.9 Empirical Mode Decomposition-LSTM

In thermal cycling tests, the extracted lower IMFs looks likes noise ,this can be prevented by raising the threshold of the mean of the signal and higher IMFs be the trend. Lower IMFs can be denoised and Higher IMFs can be de-trended. Detrending the time series can done by subtracting the selected IMFs. It can be shown that the method of empirical mode decomposition can be used to remove the trend from the raw data. EMD allows processing non linear and non stationery signals, since it doesnot require any a priory data about the signal since the trend is extracted from the signal itself.

Figure 5.30(a) shows Actual Rate Vs Predicted Rate (Train data) of the Second thermal cycle of EMD–LSTM.From figure 5.30(b) to figure 5.32(b) shows the Actual Rate Vs Predicted Rate(test data) of first,third,fourth,fifth thermal cycles of EMD–LSTM respectively.

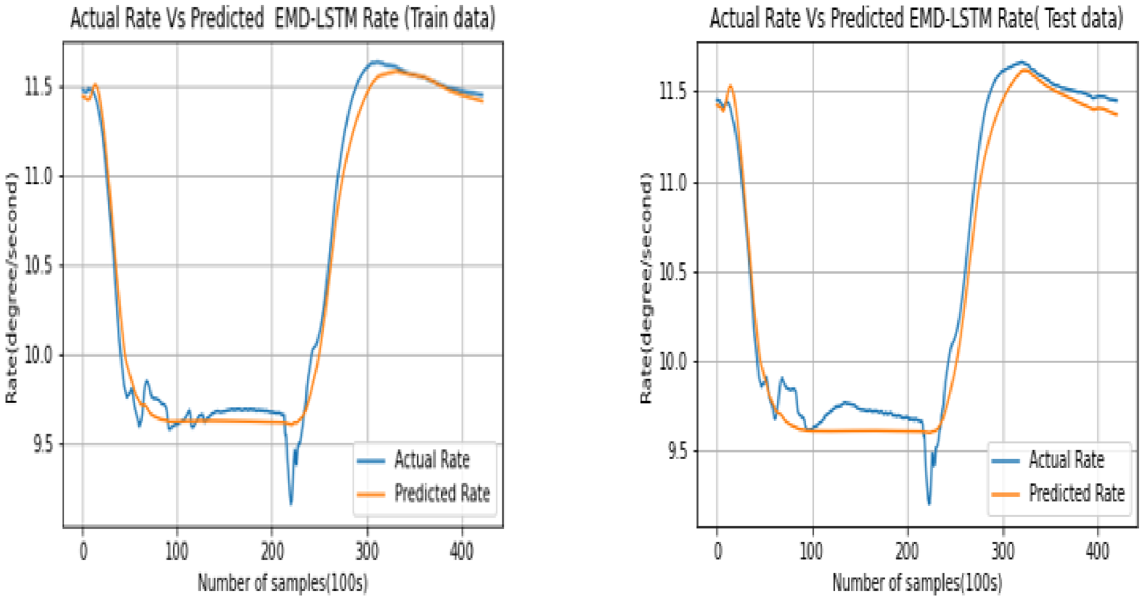

(a) Actual Rate Vs Predicted Rate of EMD-LSTM (b) Actual Rate Vs Predicted Rate of EMD-LSTM

Figure 5.65: Actual Rate Vs EMD-LSTM Predicted Rate of second and third thermal cycle.

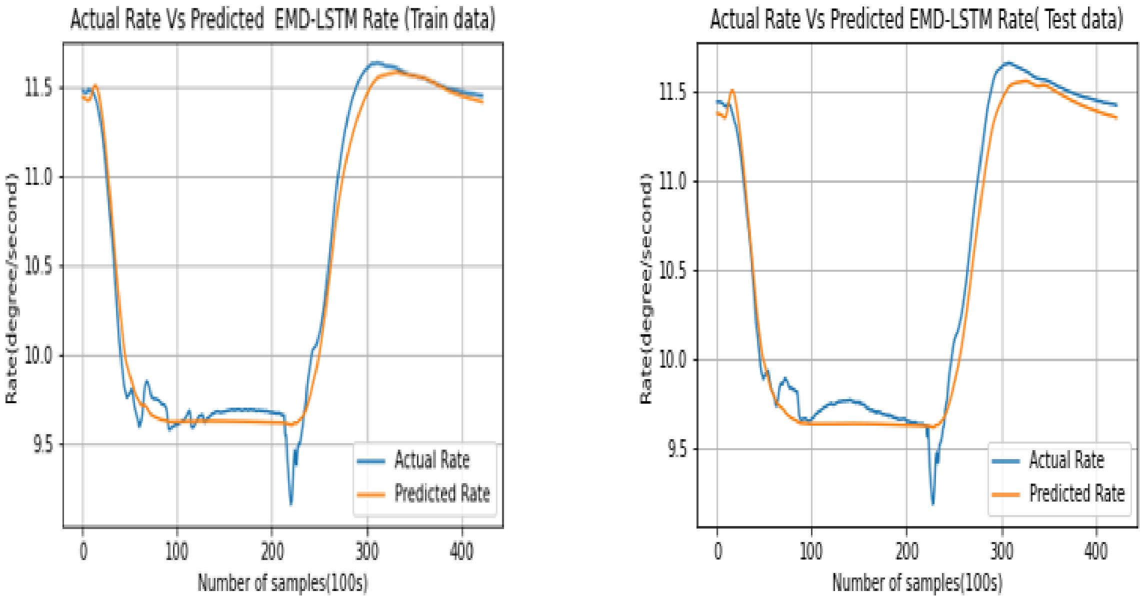

(a) Actual Rate Vs Predicted Rate of EMD-LSTM (b) Actual Rate Vs Predicted Rate of EMD-LSTM

Figure 5.66: Actual Rate Vs EMD-LSTM Predicted Rate of second and fourth thermal cycle.

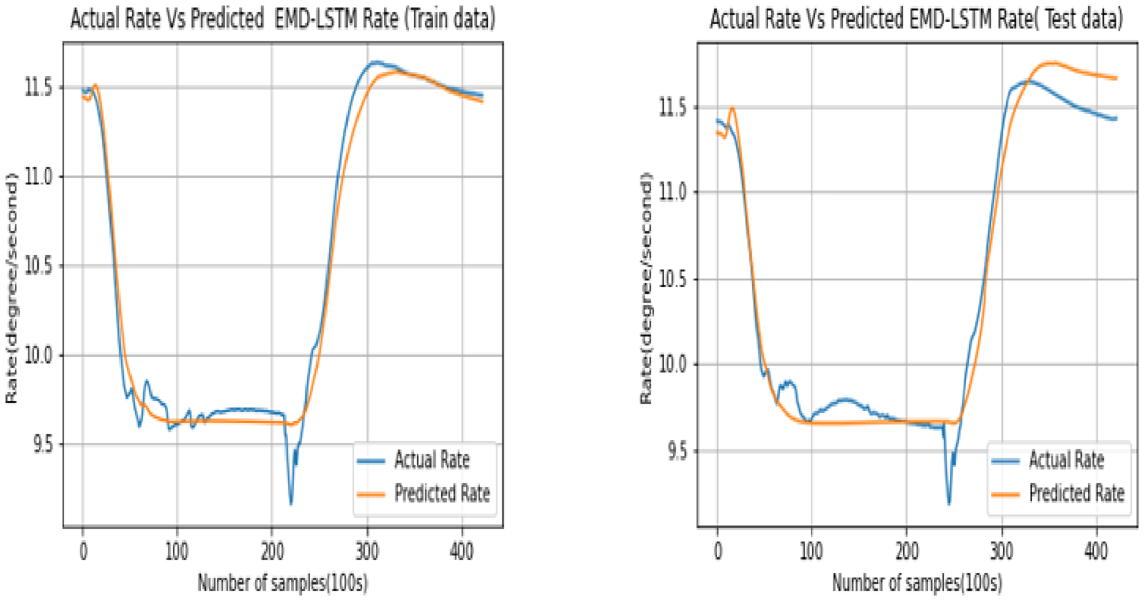

(a) Actual Rate Vs Predicted Rate of EMD-LSTM

(b) Actual Rate Vs Predicted Rate of EMD-LSTM

Figure 5.67: Actual Rate Vs EMD-LSTM Predicted Rate of second and fifth thermal cycle.

Table 5.4: Comparison of models for second and first thermal cycles

Model	Std.dev of uncomp (Train data)	Std.dev of compen (Train data)	Std.dev of uncomp (Test data)	Std.dev of compen (Test data)
LSTM	0.880604	0.147574	0.897713	0.190569
EMD-LSTM	0.876334	0.099067	0.893666	0.103604
SD-LSTM	0.875904	0.97571	0.890721	0.88972

Table 5.5: Comparison of models for second and first thermal cycles

Model	Train percentage	Test percentage
LSTM	83.241674	78.771698
EMD-LSTM	88.695339	88.406838
SD-LSTM	88.8605	90.011184

From table 5.4,table 5.5,table 5.6 ,table 5.7 shows the Comparison of three methods including LSTM, Seasonal decomposition-LSTM(SD-LSTM), EMD-LSTM of second and first thermal cycles,second and third thermal cycles,second and fourth thermal cycles,second and fifth thermal cycles respectively.

Table 5.6: Comparison of models for second and third thermal cycles

Model	Std.dev of uncomp (Train data)	Std.dev of compen (Train data)	Std.dev of uncomp (Test data)	Std.dev of compen (Test data)
LSTM	0.880604	0.14948	0.85565	0.143805
EMD-LSTM	0.876334	0.0976	0.852084	0.107342
SD-LSTM	0.875904	0.094851	0.851473	0.099561

Table 5.7: Comparison of models for second and third thermal cycles

Model	Train Percentage	Test Percentage
LSTM	83.0252	83.1935
EMD-LSTM	88.8520	87.4552
SD-LSTM	89.1710	88.3071

Table 5.8: Comparison of models for second and fourth thermal cycles

Model	Std.dev of uncomp (Train data)	Std.dev of compen (Train data)	Std.dev of uncomp (Test data)	Std.dev of compen (Test data)
LSTM	0.003545	0.000392	0.003244	0.000740
EMD-LSTM	0.003545	0.000343	0.003363	0.000481
Seasonal-LSTM	0.003537	0.000498	0.003237	0.000666

Table 5.9: Comparison of models for second and fourth thermal cycles

Model	Train Percentage	Test Percentage
LSTM	83.2909	84.4600
SD-LSTM	89.2814	88.2510
EMD-LSTM	88.8492	87.8572

Table 5.10: Comparison of models for second and fifth thermal cycles

Model	Std.dev of uncomp (Train data)	Std.dev of compen (Train data)	Std.dev of uncomp (Test data)	Std.dev of compen (Test data)
LSTM	0.880604	0.117395	0.836121	0.183315
EMD-LSTM	0.876334	0.098775	0.835036	0.148224
SD-LSTM	0.875904	0.094359	0.830177	0.13487

Table 5.11: Comparison of models for second and fifth thermal cycles

Model	Train Percentage	Test Percentage
LSTM	86.6688	78.075
EMD-LSTM	88.7286	82.2493
SD-LSTM	89.227	83.4604

5.10 Summary

This chapter deals with the visualisation,results of various Correlation and their comparisons,results of time Series Seasonal decomposition,EMD,LSTM alone,Seasonal decomposition-LSTM,EMD-LSTM of the multiple thermal cycle performance analysis data of Tuning Fork Gyroscope and these are compared to obtain the method with better performance in bias compensation.Next chapter deals with the conclusion and Future scope.

Chapter 6

CONCLUSION

This work aims to improve the accuracy of measuring angular velocity by implementing control strategies and compensation methods to overcome errors in gyroscope measurements. The focus is on the bias compensation of a tuning fork gyroscope, and this paper proposes a hybrid model that combines Seasonal decomposition-LSTM and EMD-LSTM for predicting and compensating biases. The study shows that LSTM neural networks are well-suited for forecasting bias compensation in gyroscopes, and the EMD-LSTM hybrid prediction model outperforms the single LSTM prediction model. The proposed methods offer a powerful means of improving sensor performance and accuracy, and the EMD-LSTM model is effective in improving the accuracy of TFG sensor performance.

REFERENCES

[1] S. Hochreiter and J. Schmidhuber, “Long short-term memory,” *Neural computation*, vol. 9, no. 8, pp. 1735–1780, 1997.

[2] N. Mao, J. Xu, J. Li, and H. He, “A lstm-rnn-based fiber optic gyroscope drift compensation,” *Mathematical Problems in Engineering*, vol. 2021, 2021.

[3] Q. Chen, D. Wen, X. Li, D. Chen, H. Lv, J. Zhang, and P. Gao, “Empirical mode decomposition based long short-term memory neural network forecasting model for the short-term metro passenger flow,” *PloS one*, vol. 14, no. 9, p. e0222365, 2019.

[4] Y. Rong and S. Gao, “Adaptive filtering method based on emd,” in *2018 International Conference on Network, Communication, Computer Engineering (NCCE 2018)*. Atlantis Press, 2018, pp. 671–674.

[5] X. Chen and C. Shen, “Study on temperature error processing technique for fiber optic gyroscope,” *Optik*, vol. 124, no. 9, pp. 784–792, 2013.

[6] R. Song, X. Chen, C. Shen, and H. Zhang, “Modeling fog drift using back-propagation neural network optimized by artificial fish swarm algorithm,” *Journal of Sensors*, vol. 2014, 2014.

[7] N. Li, J. Chen, Y. Yuan, Y. Han, and X. Tian, “Compensation of fog temperature drift based on ls-svm modeling,” in *2016 35th Chinese Control Conference (CCC)*. IEEE, 2016, pp. 5515–5518.

[8] G. Xu, W. Tian, and L. Qian, “Emd-and svm-based temperature drift modeling and compensation for a dynamically tuned gyroscope (dtg),” *Mechanical Systems and Signal Processing*, vol. 21, no. 8, pp. 3182–3188, 2007.

[9] B. Cui and X. Chen, "Improved hybrid filter for fiber optic gyroscope signal denoising based on emd and forward linear prediction," *Sensors and Actuators A: Physical*, vol. 230, pp. 150–155, 2015.

[10] K. Bandara, R. J. Hyndman, and C. Bergmeir, "Mstl: a seasonal-trend decomposition algorithm for time series with multiple seasonal patterns," *arXiv preprint arXiv:2107.13462*, 2021.

[11] M. Zhang and G. Wei, "An integrated emd adaptive threshold denoising method for reduction of noise in ecg," *Plos one*, vol. 15, no. 7, p. e0235330, 2020.

[12] C. Liu, Z. Yang, Z. Shi, J. Ma, and J. Cao, "A gyroscope signal denoising method based on empirical mode decomposition and signal reconstruction," *Sensors*, vol. 19, no. 23, p. 5064, 2019.

[13] C. Shen, H. Cao, J. Li, J. Tang, X. Zhang, Y. Shi, W. Yang, and J. Liu, "Hybrid de-noising approach for fiber optic gyroscopes combining improved empirical mode decomposition and forward linear prediction algorithms," *Review of Scientific Instruments*, vol. 87, no. 3, p. 033305, 2016.

[14] A. El-Rabbany and M. El-Diasty, "An efficient neural network model for de-noising of mems-based inertial data," *The Journal of Navigation*, vol. 57, no. 3, pp. 407–415, 2004.

[15] R. B. Cleveland, W. S. Cleveland, J. E. McRae, and I. Terpenning, "Stl: A seasonal-trend decomposition," *J. Off. Stat*, vol. 6, no. 1, pp. 3–73, 1990.

[16] Q. Wen, J. Gao, X. Song, L. Sun, H. Xu, and S. Zhu, "Robuststl: A robust seasonal-trend decomposition algorithm for long time series," in *Proceedings of the AAAI Conference on Artificial Intelligence*, vol. 33, no. 01, 2019, pp. 5409–5416.